UNIVERSIDADE D
COIMBRA

SEPTIAN SIGIT SETIAWAN

THE EFFECT OF USING SELF-LUBRICATING COATINGS CONTAINING TRANSITION METAL DICHALCOGENIDES IN LUBRICATED CONTACTS

VOLUME 1

Dissertation under the Joint European Master's Degree in Surface and Interfaces supervised by Dr. Todor Vuchkov and Professor Albano Cavaleiro presented to the Department of Mechanical Engineering of Faculty of Science and Technology of the University of Coimbra

July 2022

The effect of using self-lubricating coatings containing transition metal dichalcogenides in lubricated contacts

Submitted in Partial Fulfilment of the Requirements for the Degree of European Joint European Master in Tribology of Surfaces and Interfaces.

O efeito do uso de revestimentos autolubrificantes contendo dicalcogenetos de metais de transição em contactos lubrificados

Author:

SEPTIAN SIGIT SETIAWAN

Advisor[s]:

Dr. Todor Vuchkov

Professor Albano Cavaleiro

Jury:

President	**Professor Bruno Trindade**
	Professor at the Universidade de Coimbra
Vowel	**Professor João Oliveira**
	Professor at Universidade de Coimbra
Advisor	**Dr. Todor Vuchkov**
	Researcher at Instituto Pedro Nunes

Coimbra, July, 2022

ACKNOWLEDGEMENTS

First and foremost, I would acknowledge and my warmest thanks to those who contributed to completing this thesis work.

Firstly, I would like to express my gratitude to my advisors, Dr. Todor Vuchkov from Intituto Pedro Nunes (IPN) and Professor Albano Cavaleiro from the University of Coimbra, for their guidance, valuable input and tiredness support during this project. In addition, Thanks to staffs from IPN for the help in technical support.

Many and special thanks to the Tribos+ consortium especially to the coordinators (Professor Ardian Morina, Professor Mitjan Kalin, Professor Bruno Trindade and Professor Nazanin Emami) for giving this wonderful opportunity and to the European Commission's funding.

Thanks to my fellow classmates for their companion during the difficult time. To my parents and family back home who always give me support and love. To my second families in Leeds, and Coimbra who always helped me in any situation and special thanks to my second family in Ljubljana, mas Rio and his family, mbak Cecil and her family, Matija and his family and friends and others that I cannot mention one by one who always welcome, support, and encourage me when I was in Ljubljana.

ABSTRACT

This study aims to monitor the response of C-alloyed TMD coatings lubricated with oil at different testing temperatures (100 ºC and room temperature (RT)). The C-alloyed TMD coatings were successfully deposited with different carbon contents of 35.5 at. % and 45.6 at. %. Higher carbon content contributed to the change of morphology, increase of hardness, formation of amorphous structure, and to the presence of a denser and more compact structure. As for the tribological performance, for lubricated contacts, the coating with the highest carbon content showed the lowest coefficient of friction (CoF), of ~0.10 at 100 ºC, and the lowest specific wear rate, of ~9.4 x 10^{-9} mm^3/Nm. The same coating, in dry condition at 100 ºC, showed an increased of the CoF to ~0.015 at ~55.000 cycles, and a high specific wear rate of 1.4 x 10-7 mm^3/Nm. At room temperature, the coating rapidly delaminated, leading to a sharp increase in CoF and to a specific wear rate of ~2.9 x 10^{-6} mm^3/Nm for only ~20.000 cycles elapsed. Therefore, in these high carbon content coatings, limited tungsten disulphide is present at the interface, which presents an obstacle to the formation of a tribofilm in the sliding contact. Consequently, the initial friction force is considerably high, and this leads to the delamination of the coating surface.

Keywords: Carbon-alloyed TMD coating, coefficient of friction, specific wear rate, lubricated condition, dry condition.

RESUMO

Neste trabalho foram desenvolvidos revestimentos de dicalcogenetos de metais de transição (TMD) dopados com carbono para aplicações que exigem baixo atrito e desgaste reduzido, em ambientes terrestres e não terrestres. É possível encontrar na literatura estudos sobre revestimentos de carbono tipo diamante (DLC) contendo tungsténio em condições de lubrificação; tais estudos são bastante menos frequentes para revestimentos à base de TMD. Este estudo almeja monitorizar a resposta de revestimentos TMD ligados com C quando testados tribologicamente à temperatura ambiente (RT) e a 100 ºC. Os revestimentos foram depositados com diferentes teores de carbono de 35,5 % at. e 45,6 % at.. O maior teor de carbono contribuiu para a alteração da morfologia, aumento da dureza, formação de estrutura amorfa e para a presença de uma morfologia mais densa e compacta. Quanto ao desempenho tribológico em contacto lubrificado, o revestimento com maior teor de carbono apresentou o menor coeficiente de atrito, de ~0,10 a 100 ºC, e a menor taxa de desgaste específico de ~9,4 x 10^{-9} mm^3/Nm. O mesmo revestimento, em condição de contacto sem lubrificação a 100 ºC, revelou um aumento do CoF para ~0,015, num ensaio de duração de ~55000 ciclos, e uma alta taxa de desgaste específico de 1,4 x 10^{-7} mm^3/Nm. À temperature ambiente, o revestimento delaminou imediatamente para apenas ~20000 ciclos decorridos, levando a um aumento do CoF e da taxa de desgaste específica, esta de 2,9 x 10^{-6} mm^3/Nm,. Nestes revestimentos de alto teor de carbono, a quantidade de bissulfureto de tungsténio presente na interface é limitado, o que representa um obstáculo à formação de um tribofilme no contacto deslizante. Consequentemente, a força de atrito inicial é consideravelmente alta e isso leva à delaminação da superfície do revestimento.

Palavras-chave: TMD ligado com carbono, CoF, taxa de desgaste específica, contato lubrificado, contato não lubrificado.

TABLE OF CONTENTS

[LIST OF FIGURES]

[LIST OF TABLES]

[LIST OF SIMBOLS] AND [ACRONYMS/ ABBREVIATIONS

[List of Symbols]

at. % - atomic percent

K_α – an X-Ray energy at K shell

L_{cx} – Critical load at x

Wq – planimetric cross sectional wear

Wv.flat – wear volume at flat surface

2θ – the angle of detector position from the incident angle

[Acronyms/Abbreviations]

TMD – Transition Metal Dichalcogenides

DLC – Diamond Like Carbon coatings

DC – Direct Current

M – Metal element

X – Chalcogen element

MX_2 – Metal Chalcogen substance

T0 phase – A distorted metal atoms

MoS_2 – Molybdenum (di)sulphide

WS_2 – Tungsten (di)sulphide

$MoSe_2$ – Molybdenum (di)selenide

WSe_2 – Tungsten (di)selenide

Ti – Titanium element

C – Carbon element

N – Nitrogen element

TSD – target-to-substrate distance

S/W ratio – Sulphur to Tungsten ratio

Al – Aluminium element

Au – Aurum (gold) element

Pb – Plumbum (lead) element

Ni – Nickel element

Cr – Chromium element

PVD – Physical Vapor Deposition

IBAD – Ion Beam-Assisted Deposition

RF – Radio Frequency

UBS – Unbalanced Magnetron Sputtering

HIPPMS – High-power impulse magnetron sputtering

TMD-C – Transition Metal Dichalcogenides alloyed with Carbon element

IFL – Inorganic Fulleren Like

MoDTC – Molybdenum dithiocarbamates

OFM – Organic Friction Modifier

ASTM – American Society for Testing and Materials

DIN – Deustchex Institut fur Normung

100Cr6 – a type of carbon chromium material

Ra – arithmetic average of surface heights measured across a surface

SRV – Schwingung Reibung Verschleiß

µm – micrometer

IPN – Instituto Pedro Nunes

W-S-C coating – tungsten suplhur carbon coating

Ar^+ ion – Argon element ion

W/cm^2 - watt/cm squared

V – Volt

Min – Minute

SEM – Scanning Electron Microscope

XRD – X-Ray Diffraction

MRD – Malvern Panalytical X'Pert

kV - kilovolt

mA - millivolt

ICDD - International Center for Diffraction Data

mN – miniNewton

N – Newton

L_{c1},L_{c2}, L_{c3} – Critical Loads (1,2,3)

SAE – Society of Automotive Engineers

5W30 - a type of oil for winter that has low temperature viscosity and 30 is the high temperature at 100 degrees

RT – Room Temperature

Hz – Hertz

mm – milimeter

m/s - meter/second

WDS - Wavelength-Dispersive X-Ray Spectroscopy

CHAPTER 1

1. INTRODUCTION

The traditional form of tribology has been recorded since early human life. There are numerous documented examples of early civilizations developing bearings and low-friction surfaces. Tribology is a new field of science defined in 1967 by an Organization for Economic Cooperation and Development Committee. It focuses on the friction, wears, and lubrication of interacting surfaces in relative motion. Wear is the leading cause of material waste and mechanical performance loss, and any reduction in wear can result in significant savings. Therefore, reducing friction and controlling wear can be achieved by performing lubrication. Tribology applies operational analysis to major economic issues such as the reliability, maintenance, and wear of technical equipment ranging from household appliances to spacecraft. Then, the critical question comes up: Why are the interacting surfaces in relative motion (basically rolling, sliding, typical approach, or separation of surfaces) crucial to our economy, and how do they affect our standard of living. The answer is that virtually every device's operation is dictated or controlled by surface interaction [1].

A general conclusion from numerous experiments and theories is that tribology is the study of:

1. The properties of films of the contacting bodies
2. The consequences of a film’s failure or absence, usually characterized by high friction and wear.

Film formation between any sliding objects is formed naturally without the intervention of a human. Film formation could be the primary mechanism that prevents exceptionally high shear rates at the interface of two rigid sliding objects. A thin film is mechanically stable, making it difficult to expel such a film by squeezing between two objects completely. Some of the films can be squeezed out easily, but to remove them completely is nearly impossible. Although sliding is destructive to these films, causing wear, it also facilitates their replenishment by introducing a 'lubricant' or the formation of new film

material from wear particles. The principle of tribology is to minimize the two main drawbacks of solid-to-solid contact: friction and wear, but this is not always the case. As illustrated in **Figure 1**, it is preferable to minimize friction while maximizing wear, or to minimize wear while maximizing friction, or to maximize both friction and wear. For example, in brakes and lubricated clutches, reducing wear but not friction is desirable [1].

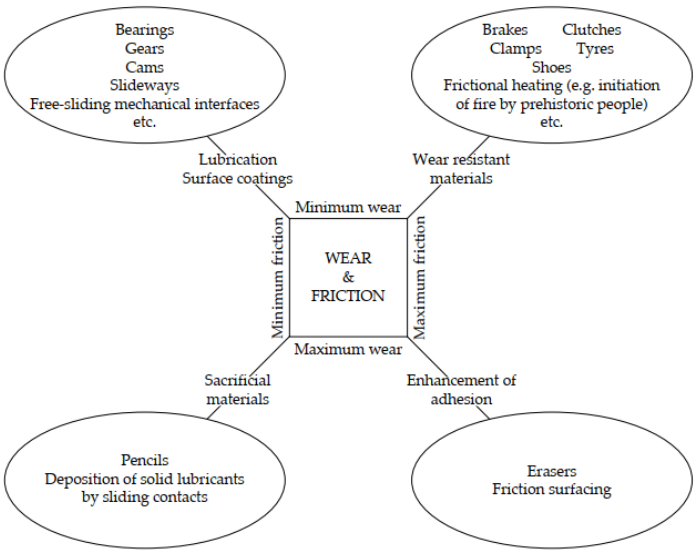

Figure 1.1 Practical objectives of tribology [1].

In some industrial applications, such as in the aerospace industry for transport, networks, and the field of space exploration, depending on the efficient operation and service life of aircraft, satellites, spaceships, etc., controlling friction and wear is essential because space machinery must operate in both terrestrial and non-terrestrial environments, where contamination in liquid lubrication may become the main issue. Therefore, solid lubricants have increased the demand for the alternative of liquid lubricants. The use of self-lubricating coatings is the recent transition of cutting and milling machining from the use of liquid lubricants or coolants to dry machining that is deemed to protect the environment and to eliminate the costs for coolant. It also presents the thermally stable machining tools in high temperatures with hard and good wear resistant surfaces. [2] Over the last few decades, various materials have been developed to build solid lubricant coatings. A popular subset of solid lubricants that meet the needs of the space industry is innovative self-adaptive coatings like Transition Metal Dichalcogenides (TMDs) have paid a lot of attention due to low Coefficient of Friction. CoF reaches less than 0.03 in dry, vacuum environment [2,3]. Recently, the addition (alloy) of nitrogen and carbon has been introduced to achieve better

hardness and wear resistance. Due to the crystal structure difference between alloyed TMD coatings and the coated substrates, the introduction of another element such as chromium (Cr) as an interlayer between alloyed TMD coating and the substrates provide an advantage in adhesion properties [3]. There are numerous opportunities to expand the use of self-lubricating TMD coatings by advancing their structure. The success using hard coating in dry machining clearly provides some benefits in energy and cost savings. There is still homework to expand the use of solid lubricants to energy dissipating mechanical contacts, for example, bearings, gears, rails etc. Lately, the research is limited in the minimization of contact oxidation and structure evolution process (e.g., ambient or space) [2]. It is clearly seen that the use of self-lubricating coatings is generally found in dry contact. On the other hand, the research on lubricated contact is lack of attention. Therefore, this study will analyze the synergy between solid coatings and oil lubricant to observe the friction and wear properties.

1.1. THESIS OBJECTIVES

The proposed thesis is to contribute in the development of transition metal dichalcogenide as self-lubricating coatings by alloying with carbon (C) in different composition. In this study, bearing steel materials generally used for bearing balls will be used as the substrates. Therefore, depositing chromium layer is also considered to improve the adhesion between TMD coatings and substrates. Some literatures studied the synergy of Tungsten contained Diamond Like Carbon (DLC) coating in the lubricated condition. On the other hand, less literature observed the use of TMD solid lubricant in the lubricated contact. Thus, introducing lubricants will be assessed during tribological assessment of C alloyed TMD coatings. Moreover, the properties of coatings such as morphology, structure, mechanical and adhesion will be observed during this research work.

To achieve the success of this thesis, the following objectives will be developed into some sub-objectives as follows:

1. Analyze the effect of different supplied power to the deposition of Carbon alloyed TMD coatings.
2. Understand the alteration of coefficient of friction (CoF) and specific wear rate in the varied testing temperatures.

3. Investigate the influence of additional formulated engine oil in the tribological performance whether the oil lubricant will work synergistically or antagonistically with the presence of self-lubricating coating

1.2. THESIS ORGANIZATION

This thesis draft is consisting of 6 chapters. ***Chapter 1*** shows the introduction of the needs of tribology, lubrication, and solid lubricants using TMD followed by an overview of TMDs with the objective of this thesis. ***Chapter 2*** focuses on the detailed information about TMD coatings, its properties, the development of alloyed TMD, tribo film formation in lubricated contact and research gaps. ***Chapter 3*** covers the preparation of materials used for substrate, the preparation of deposition technique and preparation of characterization methods. ***Chapter 4*** presents and discusses the results with detail information along with literature comparison. ***Chapter 5*** sums up the findings of this research work. Potential future work is presented in ***Chapter 6.*** Finally, ***Chapter 7*** is dedicated to literatures cited to compose this thesis.

CHAPTER 2

2. STATE OF ART

This section is dedicated to presenting the understanding of transition metal dichalcogenides in the present work, which is the main topic of this project. The work will include properties, structure, fabrication methods, tribological performance, and the synergy of the solid coating with the presence of oil lubricants in detail. This thesis project also delves into relevant past and current research information.

2.1. TRANSITION METAL DICHALCOGENIDES

For decades, transition metal dichalcogenides (TMD) have been studied for their excellent self-lubricant properties in dry air or vacuum. They provide good mechanical properties under similar conditions, making them suitable for replacing other hard coatings in applications requiring low friction. But there are some conditions where TMD films' mechanical properties deteriorate quickly, making them unsuitable for the specific application, such as high-load terrestrial (open atmosphere) applications. A successful method to reach good tribological properties of TMD coating is by alloying with carbon, improving mechanical and tribological properties [4]. Thus, understanding the details about TMD and how its structure affects the tribological properties and mechanical properties, especially hardness, is mandatory in this study. This study will discuss TMD's structure, properties, and tribological performance in detail.

2.1.1. STRUCTURE

The structure of TMD exists in two crystal forms, hexagonal and rhombohedral. The most common and important is in hexagonal structures in low friction applications [5]. Chao et al. [7] describe the composition of TMD layered material consisting of a transition metal layer (M) in which each unit (MX_2) is sandwiched between two chalcogens (X) atomic layers. The arrangement of the atoms depends on the structure of the 2D TMD which can be categorized into a triangular prism (hexagon, H), an octahedron (tetragonal, T), and their distorted phases (T0), as shown in **Figure 2.1** (a) In the H-phase material, each metal atom shows six branches into two tetrahedra in the + z and z directions, but in the top view you

can see the hexagonal symmetry **Figure 2.1** (b) Metal atoms are further distorted (or dimerized in one direction), called the T0 phase which changes the atomic displacement of chalcogen atoms [7].

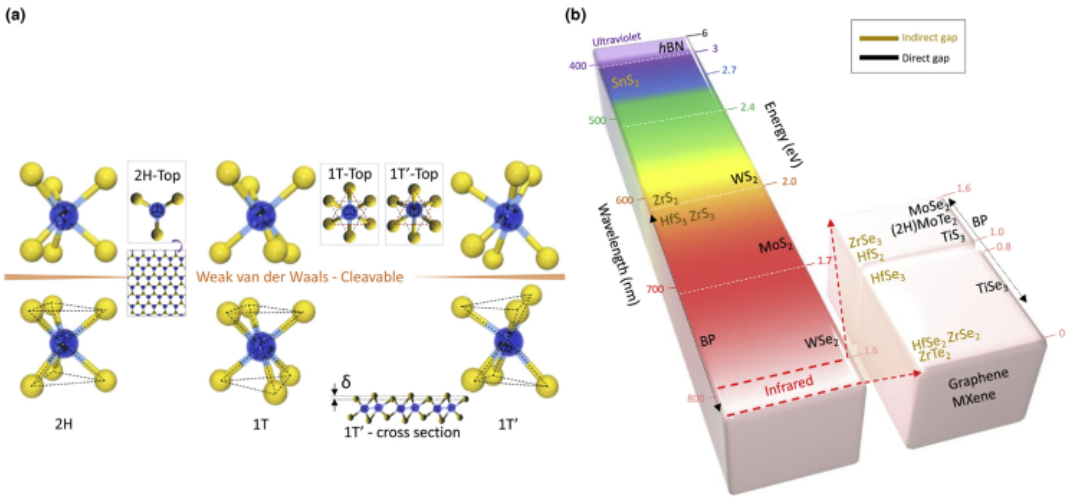

Figure 2.1 (a) Structure of layered TMD and (b) Bandgap of 2D layered materials [6].

The self-lubricant properties of TMD combine strong intra-planar bonds between chalcogenide and metal atoms with weak bonding between adjacent metal-chalcogenide layers. As a result, the inter-lamellar bonds are easily broken, allowing for sliding, while the intra-planar bonds help to resist asperity penetration [7].

On the other hand, the TMD crystal is ideal for sliding in vacuum or non-reactive gases. In contrast, oxygen or air humidity is detrimental, resulting in high friction and wear rates. As a result, the columnar morphology and porous structure of sputtered TMD films severely limit the property of self-lubricant coating in humid air [5]. When developing novel self-lubricant TMD-based films, researchers should consider the microstructure of the self-adapting coating to the sliding process in order to achieve the desirable properties, especially tribological properties.

2.1.2. PROPERTIES

TMD as self-lubricating material in this study is solely focused on solid lubricant (TMD coatings). The properties of solid lubricant will be explained in detail in this section. Understanding the mechanism of metallic friction is necessary to deepen the information on

how the solid lubricant works. Friction is not the effect of contacting surface, but penetration and distortion happen in some depth under the surface. Then the bulk properties of metals play a role in the frictional and the nature of sliding. The physical properties of metals, such as hardness melting point, contribute to the nature of sliding and friction values. The frictional resistance of unlubricated metals is mainly caused by the shearing of metallic junctions as the effect of adhesion and welding on the point of contact and dragging or ploughing the irregular surface of the harder metals to the metals that have soft hardness [8]. The shear strength of TMD parallel to the sliding planes is reported very weak between the sandwich layers and it is the reason why TMD is used for solid lubricants. Because of its unique highly anisotropic crystal structure, the coefficient of TMD coatings can reach as low as 0,001 but loss of friction coefficient can be found. To achieve a low friction, adhesive forces between the coatings and solid substrates have to be higher than the weak attractive forces between lamellae leading to the occurrence of slip and resulting to low friction coefficient [5]. Thus, the properties of TMD depends on its structure. In this study, the properties of TMD solid lubricants will describe on the tribological properties, mechanical properties and adhesion.

2.1.2.1. TRIBOLOGICAL PROPERTIES

For most tribological applications, protecting the bulk material with a thin layer is an excellent way to improve wear resistance. The development of transition metal dichalcogenides, such as MoS_2, WS_2 $MoSe_2$, WSe_2, and so on, has been known since the late 1920s as coating materials [9]. Especially for MoS_2 and WS_2 in the form of nanotubes has been taken advantage of TMD as additives on lubricating oils serving promising tribological properties. Unfortunately, most liquid lubricants show their limit in space application under various operating conditions (temperature, humidity, pressure, and radiation) [10].

The use of MoS_2 and WS_2 studied as thin coating starting from Earth [11] to the outer area for space applications started in the 1960s [12] until the present days [2,13,14]. It is also subjected to a huge variety of running conditions. For example, some liquid lubricants limit the high vapor pressure applications. Thus, a thin solid coating becomes the solution. Another method used by researchers is ionic liquids that serve adequate tribological performance. Still, it comes with a disadvantage which is fragile to tribo-corrosion [15],

toxicity [16], rapid decomposition [17], and limited temperature range [17]. On the other hand, most solid lubricants show significant features in lowering friction in adjunct with the increase of contact stress. The self-lubricating properties come on the surface in a low shear transfer film when the surface materials contact the counter body, usually formed by tribo-chemical reactions on the surface [18].

2.1.2.2. ADHESION

The properties of TMD coatings are dependent on its composition, structure and morphology. These parameters will affect its durability. Some findings show the low durability of TMD material, such as MoS_2 on titanium alloys. The adhesion was reported too low, and it also happens in some metals as the substrates. For example, sputtering of MoS_2 onto some metals (copper, silver, etc.) resulted in poorly adherent films and bad durability [13]. Other TMD materials show similar properties to MoS_2, but they don't provide better tribological properties. For example, pure niobium disulphides and diselenides provide poor lubrication properties because their electron structures are different from the structures that MoS_2 has. Another example comes from sputtered tellurides. The coating layers are not bonded strongly on steels because of limited adhesion [19].

2.1.2.3. MECHANICAL PROPERTIES

In some studies, TMD coatings show improvement not only in tribological performance but also in its mechanical properties. In some studies [5,20,21], carried out with pure TMD coating, the recorded hardness fluctuated in the range of 0.3 and 2 GPa. The mechanical and tribological properties of pure TMD coatings (WS_2) were improved by Shushen et al. [22,23] by modifying the microstructures. Changing structure employing the plasma's bombardment function (adjusting argon pressure) on growing films is one of the ways [21]. In Addition, some researchers have developed mechanical properties with changing TMD coatings' microstructure, for example, doping Ti into WS_2 [22] and adding C and N elements into WS_2 [23].

Research done by Hirvonen et al. [24] using MoS_2 proved the increase of nano hardness in the wear track of MoS_2 films. The structure orientation of deposited MoS_2 changed from (101) to almost exclusively (002) structure orientation. In addition, they

observed the rise of hardness in the wear track due to densification of the structure during the sliding process.

2.1.3. ALLOYING TRANSITION METAL DICHALCOGENIDES

Comprehensive studies on pure deposited TMD coatings face challenges in low load bearing capacity and limited wear resistance due to its softness and weak bond [25]. In order to improve the performance, TMD coatings were co-deposited with non-metallic interstitial elements such as nitrogen [19,26-28] and carbon [4.19,25,29-33], producing coatings whether using tungsten/molybdenum-sulfur-carbon (W/Mo-S-C) or molybdenum/tungsten-selenium-carbon (Mo/W-Se-C) that showed TMD materials alloyed with some elements provides good grasp on the improved adhesion, tribological performance and mechanical properties.

Carbon-alloyed Transition Metal Dichalcogenide (W/Mo-S-C) or (Mo/W-Se-C) coatings have been extensively used in the previous studies with some working parameters. Pimentel et al. [4] deposited tungsten disulphide coatings doped with carbon (W-S-C) by direct current magnetron sputtering, radio frequency with a reactive gas, and radio frequency with WS_2 pellets. They deducted the tribological properties and their hardness depending on the carbon content. The highest hardness has resulted in 40 at. % C (the coating had a varied carbon content from 25 to 70 at. % C. The measured nano hardness in the wear track reached about 9 GPa. The study also shows that the same value of hardness can be found in the inside of wear track and outside of wear track, which means that the sliding effect doesn't affect the mechanical properties of the coating surface.

Polcar et al. [19] found low friction in humid air coming from its self-adaptation by forming a thin tribofilm layer in the contact and sub-surface orientation of TMD platelets inside the carbon matrix. The tribological concept works as illustrated in **Figure 2.2**. In conjunction with improved tribological properties, the hardness values increase in the addition of carbon content into pure TMD materials from 0.5 GPa to ranging 2.9-9.2 GPa.

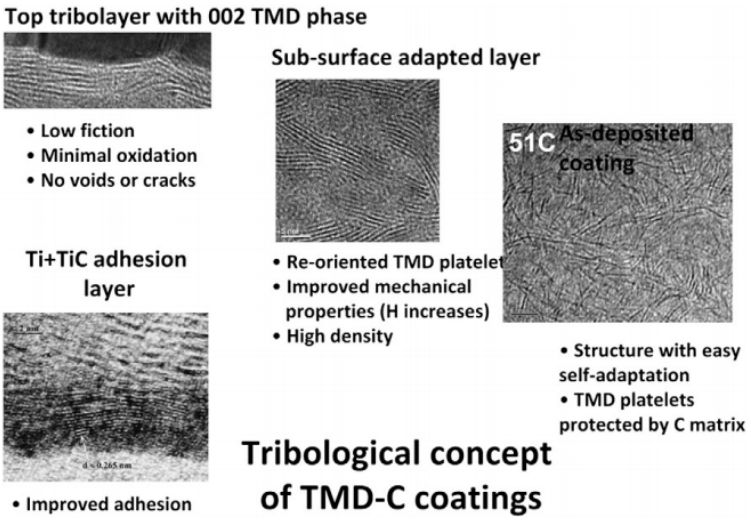

Figure 2.2. Tribological design of TMD-C films. [19]

Yaqub et al. [29] deposited Mo-S-Ce with varied carbon content. The carbon content was varied between ~44 and 60 at. %. Additionally, the effect of negative substrate bias usage was studied while keeping the carbon content at ~50 at. %. The use of substrate bias resulted in increased hardness with values up to ~5 GPa compared to ~3.5 GPa for the coatings deposited without substrate bias. The best performing coating in terms of friction and wear was deposited using the addition of negative substrate bias of 90 V DC and having a 50 at. % of C. This coating showed a CoF and specific wear rate of ~0.06 and ~2.65 × 10^{-7} mm^3/Nm, respectively.

In their work, Evaristo et al. [31] characterized W-Se-C's tribological and mechanical properties. The deposition was done with 40 W of applied power on WSe_2 target, and the power was increased up to 110 W without detrimental effect. From this experiment, they concluded that they W-Se or carbon contents affected by the power supplied on the targets. Deposited W-Se-C coatings with higher carbon content shows worse wear resistance by decreasing the friction coefficient in the increase of applied load. On the other hand, coatings with lower carbon content showed a significant decrease of coefficient of friction in the increase of applied load leading to the increase of contact pressure. Thus, it indicates that the decrease of friction with the contact pressure is commonly found in pure TMD coatings. In addition, the hardness values exhibited similar values close to 3.5 GPa with 33-56 at. % of carbon content, which is higher than pure Mo-Se coatings.

Vuchkov et al. [32] experimented on the synthesis of Mo-Se-C and W-S-C films by varying carbon content and target-to-substrate distance (TSD) of 15 cm and 25 cm. In the Mo-Se-C films deposited with TSD of 15 cm, the coefficient of friction began at 0.8. It increased slightly around 0.09-0.1, but no metal-to-metal contact was spotted in comparison with pure Mo-Se deposited at the target-to-substrate of 25 cm, which had 0.03-0.04. Still, it rose continuously until the deposited coating layer was removed. Nanoindentation was performed to observe the hardness of the substrates. The hardness increases significantly when the carbon is added to the coatings. The hardness of carbon alloyed without substrate bias around 4-5 GPa deposited at the distance of 15 and 25 cm between the target and substrate / target-to-substrate distance (TSD). It showed a higher result of 7.1 and 7.8 GPa of hardness when combined with substrate bias. The biasing substrate affects the increase of density and compactness of the coatings. As a result, it affects the increase of hardness [32]. In the W-S-C case, they deposited W-S-C coatings by closed-field unbalanced magnetron sputtering in the power control mode on the 4 targets (one graphite target of 99,99 % purity, one tungsten disulphide target of 99,99 % purity, and two carbon targets of 99,99 % purity) with 3 various TSD of 10, 15, and 25 cm. TSD provides a significant contribution in the sulphur tungsten ratio (S/W ratio). Thus, the coatings with lower S/W ratio and higher carbon content leading to denser microstructure and increased hardness. The hardness ranges from 5.27 to 7.36 GPa [33].

Even though alloying with some non-metallic elements increases the tribological properties and mechanical properties of TMD coatings, there are some disadvantages of TMD solid lubricants:

1. In some conditions, TMD is highly sensitive to environmental attacks.
2. Columnar morphology indicates that the film is highly porous microstructure, and
3. The hardness is comparably low compared to Diamond-Like Carbon (DLC) coatings [5].

Therefore, various attempts have been applied to cope with those problems. The purpose of TMD film modification is mostly to increase density, to reduce porosity, to improve adhesion, and to increase hardness by doping with metallic elements, such as Ti, Al, Au, Pb, Ni, and Cr [5]. The last element has been widely used to develop adhesion in the interfaces between the substrate (mostly steels) and TMD coatings.

2.2. PHYSICAL VAPOR DEPOSITION (PVD)

The thin-film formation explained and discussed above is deposited by Physical Vapor Deposition. This process is the atomistic process in which material is taken from vaporized solid or liquid sources in terms of atoms or molecules. The vapor is transported to the targeted substrate through the gaseous form in the vacuum or low-pressure gaseous environment. Then, it reaches the surface of the substrate it is condensated. The deposited film varies in thickness in the range of a few nanometers to thousands of nanometers. It is possible to form multilayers coatings, graded composition deposits, very thick deposits, and freestanding structures [34]. There are some main categories of the PVD process. They are vacuum deposition (evaporation), sputter deposition, arc vapor deposition, and ion plating, as illustrated in **Figure 2.3.** [34]. But the main concern of this study falls into the sputtering process. Thus, the concept and definition of sputtering will be discussed further.

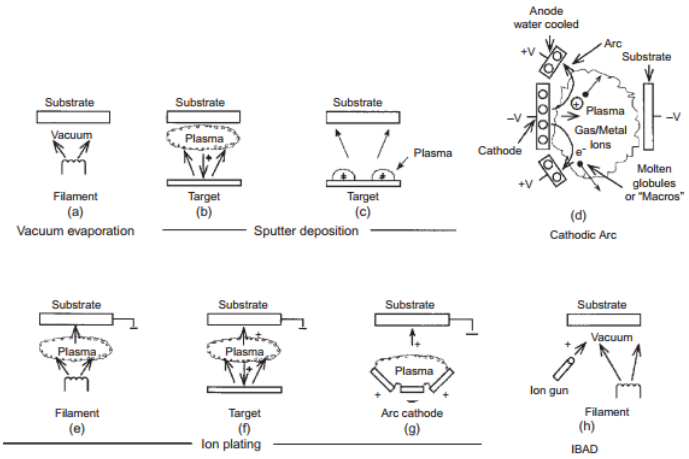

Figure 2.3. PVD techniques (1) Vacuum Evaporation, (b) and (c) Sputter Deposition in a Plasma Environment, (d) Sputter Deposition in a Vacuum, (e) Ion Plating in a Plasma Environment with a Thermal Evaporation Source, (f) Ion Plating with a Sputtering Source, (g) Ion Plating with an Arc Vaporization Source, and (h) Ion Beam-Assisted Deposition (IBAD) with a Thermal Evaporation Source and Ion Bombardment from Ion Gun [34].

2.2.1. SPUTTERING DEPOSITION

Sputter deposition is atoms originating from a sputtered surface (target). Wright described sputter deposition of films for the first time in 1877, and it was possible since sputter deposition requires a vacuum condition. In 1904, Edison patented technology for

placing gold on wax image cylinders using a sputter deposition process. Sputter deposition was not commonly employed in the industry until the need for repeatable, stable, and long-lasting vaporization sources arose, along with the introduction of several forms of magnetron sputtering. The most extensively used sputtering arrangement is planar magnetron sputtering, which uses a magnetic field to confine secondary electron motion near the planar target surface [34].

The term sputter deposition usually only refers to a surface sputtered as the source of the deposited material. Sputtering configuration can be in the form of ion beam sputtering, magnetron sputtering, unbalanced magnetron sputtering (UBS), high-power impulse magnetron sputtering (HIPPMS), radio frequency (RF) sputtering, etc. Exceptional sputtering circumstances, such as reactive sputter deposition for compound film deposition or bias sputtering, where a bias is imposed on the substrate to allow for contemporary ion bombardment of the depositing film, may be recommended in some cases [34].

The process of deposition in the vacuum chamber must follow four steps that must be fulfilled on the placement of the substrates in the vacuum chamber, as follows:
(1) The vacuum chamber must me in high vacuum condition
(2) Etching by cathodic cleaning. Ion bombardment onto the substrate from plasma etching is supposed to clean the contamination located on the surface,
(3) Deposition of the coating layer on the substrate. Some materials are primarily used, for example, titanium, zirconium, and chromium nitrides or oxides, among others [35].

2.2.2. MAGNETRON SPUTTERING

Most common studies of PVD for TMD deposition utilize some different target-power supplies; Direct Current (DC) magnetron sputtering [30-31] and Radio Frequency (RF) [30,37]. The development of sputtering process has begun in the 1600s and 1700s. Continuously, magnetron sputtering has raised an attention in the coating deposition. Mattox in his book [34] applied a magnetic field to deflect the electrons. By arranging the target surface and the magnet accordingly, the electrons circulate a closed path on the surface of the target. The high flux of electrons produces a high electron flow density plasma that can extract ions and sputter the target material. This process allows configuring magnetron sputtering configuration. **Figure 2.4.** shows some magnetron sputter configurations [34].

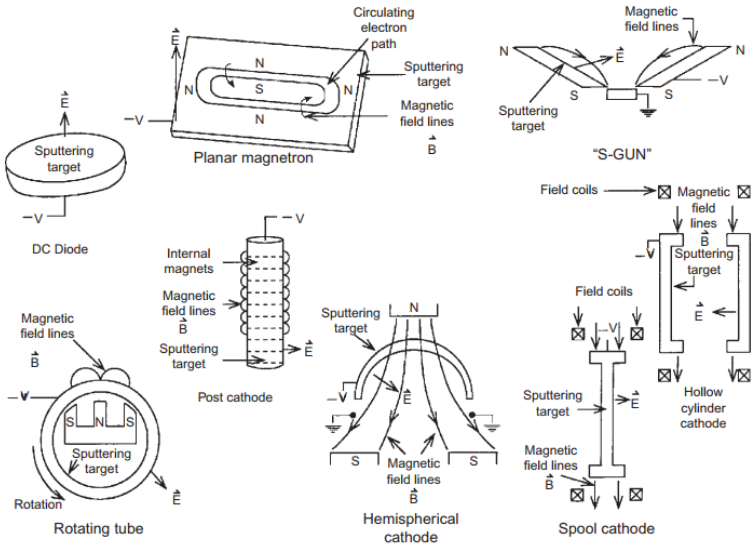

Figure 2.4. Illustration of sputtering target configuration (clockwise): Planar DC diode, planar magnetron, 'S' gun, hollow cylinder, spool, hemispherical, post, and rotating tubular magnetron [34]

The planar magnetron is frequently used as the common source of magnetron Some examples of sputtering configurations have their advantages. For example, the configuration of a planar magnetron creates a vaporization source composed of two parallel lines. The post-code source can deposit in complex shapes, such as inside a cylinder or cylindrical fixture. The hollow cylindrical cathode is mainly used to coat three-dimensional parts because the flux runs from all directions [34]. DC sputter magnetron has been used to perform nanocomposite coatings of TMD-C type. There is no clear evidence of the best method to synthesize the coatings by magnetron sputtering. This study focuses on the Direct Current magnetron sputtering, which process is shown in **Figure 2.5.** [32].

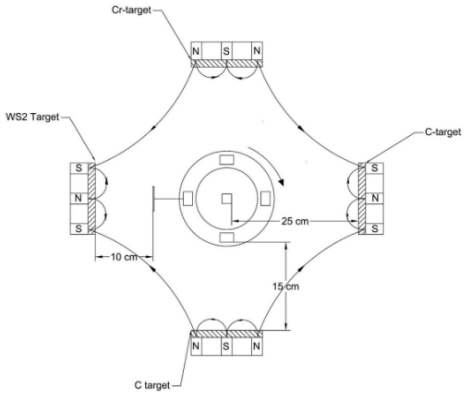

Figure 2.5. Schematic configuration of the deposition unit [32]

Yakub et al. and Vuchkov et al. [29,30,32,33,36] have successfully deposited TMD coatings using either DC or RF magnetron sputtering. Yakub et al. succeeded in optimizing the synthesis and properties of Mo-Se-C coatings in terms of a combination of low stoichiometry, high crystallinity, high hardness, and microstructure for TMD-C solid lubricants coatings [30]. DC magnetron sputtering will be employed in this study. Then, the deposited coating will be tested to measure its tribological properties on how the tribolfilm layer is formed on the contacted surfaces. This formation will also be discussed extensively.

2. 3. TRIBOFILMS FORMATION

Gustavsson et al. [37] concluded five different routes to forming the tribofilms from solid lubricants in a similar structure, composition, and tribological characters. The formations of WS_2 tribofilms come from the coatings and conditions. They explained clearly that the formation of WS_2 tribofilms go through 2 steps. Firstly, a very easy-to-shear layer is formed and secondly the layer expelled to the top surface of the harder substrate during sliding contact. As a result, an ideal combination between very low shear stress and a very small contact area to shear is formed. With different initial surface, several types of coating, materials, and fluids create similar pure crystalline WS_2 tribofilms. The first two routes mention the formation of WS_2 tribofilm without any other nanoparticles in the medium of oils or greases but with different compositions of coatings. Some problems come up from the removal of WS_2 from the coating, such as the adhesion of pure WS_2 being too low so it can be removed easily and the transfer of WS_2 to form tribofilm layer leaving the alloying elements of the coating to hinder the formation of coherent, dense transfer film. In addition, for the last three routes, the tribofilm formation with and without additional nanoparticles with the medium of oils, greases, or fuel with different compositions of coating materials. These routes will be the main topic of this thesis study. They are:

2.3.1. Starting from a metallic matrix incorporating WS_2 in the form of Inorganic Fulleren Like (IFL) nanoparticles.

This route involves the addition of inorganic fullerene-like nanoparticles of WS_2 (and MoS_2), which can be added on the contact by metallic coatings, such as electrolytic nickel coatings. During the tribological contact, exposed particles fractured, and loosed crystallizing expel onto the surface and form very similar WS_2 (or MoS_2) tribofilm. To understand the mechanism clearly, it’s better to look for how the nanoparticles work.

TMD nanoparticle has been made to replace the existence of MoDTC as an environmentally friendly organic friction modifier (OFM). In some cases, nano-balls-shaped particles will deform and rupture under high normal stresses. Thus, exfoliations of TMD particles occur. The lubricating properties of these transition metal dichalcogenides is still under further investigation how the mechanism works. Common knowledge mechanisms on these nanoparticles are postulated in three steps, namely (1) rolling of nanoparticles working as nano or micro ball bearing (2) deformation of nanoparticles leading to surface enhancement/healing, for example, filling cracks, preventing asperity contact, and (3) exfoliation and deposition of nanoparticles on to surfaces that are illustrated in **Figure 2.6**. (a), (b) and (c) respectively, [12] Nanotubes particles show better performance when exfoliation happens, but it is limited in the solubility in the base oil. Dispersants should be added to prevent coagulation of the nanotube particles. [12]

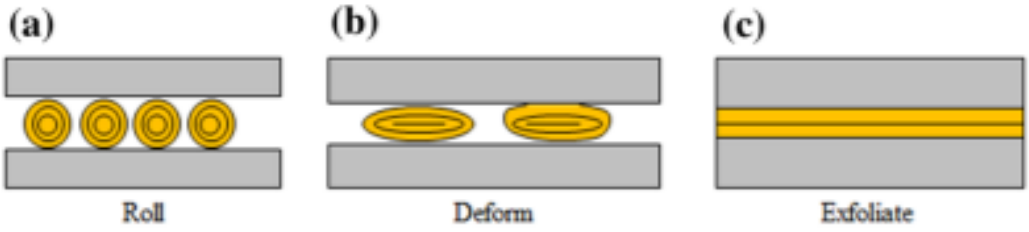

Figure 2.6. Illustration of lubrication mechanism (a) rolling, (b) deformation and (c) exfoliation [12]

The addition of nanoparticles can also be added in oils or greases, but in some cases, nanoparticles have trouble entering the contact system because of narrow inlet sliding interfaces [38]. Therefore, poor lubrication happens. Gustavsson et al., in another study, suggested that adding oil hinders tribolfim formation by preventing wear fragments from bonding the surfaces [39].

2.3.2. Starting from hard, tungsten alloyed DLC coatings and picking up sulphur from lubricating oil or fuel.

In this route, the lubricant contains sulphur-based additives, which react with W to form WS_2 film on the counter body made of steel. Thus, the friction drops. Other studies show a similar mechanism in the low suplhur content from the fuel in the tribological contact between steel coated with a tungsten containing DLC and uncoated steel. The formation of WS_2 existed on the surface of uncoated steels [40,41].

2.3.3. Starting from pure tungsten and picking up sulphur from a metastable, hard countersurface.

Tribochemically active Ti–C–S nanocomposite coatings are employed on this route. It consists of metastable S-doped titanium carbide and releases S during tribological contact sliding with steel bonding with Fe leading to lower friction. When the release S reacts with W from coating or uncoated tungsten material on the surface, it leads to WS_2 low friction tribofilm [37].

Gustavsson at al. revealed the fact that pre-deposited disulphide films cannot serve solely as low friction agent but WS_2 tribolfilms occurs as a result of friction induced self-organisation intro crystalline under various, different conditions. These conditions state that the presence of W and S exist in the interface region that has been discussed above. The mechanism involving oils/greases/fuels into the tribological contact between TMD coatings and steel/tungsten bodies is shown in the **Figure 2.7**. (a), (b), and (c) [37].

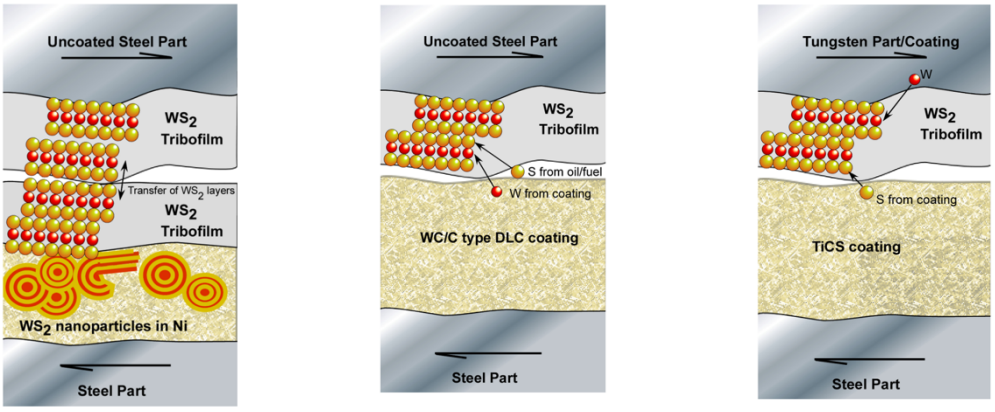

(a) (b) (c)

Figure 2.7. Routes of WS_2 formation (a) additional Fullerene-like WS_2 nanaoparticles, (b) W-containing DLC coating and extracted S from oil/fuel additives, (c) reaction of extracted S from the metastable nanocomposite TiC_xS_y coating [37].

CHAPTER 3

3. METHODOLOGY

In this section, the author will present the detailed methodology used in the synthesis of TMD coatings using magnetron sputtering, the instruments used during the experimental and the parameters to characterize the coatings.

3. 1. PREPARATION OF THE SUBSTRATES

The materials used on these experiments are disks made of a high-quality alloy steel with standard DIN 100Cr6 that is usually applied for bearings. It is prepared into some coupons in order to make it easily deposited and tribologically tested (ball-on-disk tests) with dimension $\emptyset = 24\,mm$. Balls made of DIN 100Cr6 are used with $\emptyset = 10\,mm$ and silicon wafers are also prepared and deposited for the purpose of coating thickness measurements. Firstly, the disks go through surface preparation following the standard ASTM D-5707 for tribological properties test using a Linear-Oscilation (SRV) test machine. The surface must meet the requirements of surface finish 0.45 μm < Ra > 0.050 μm. It can be done by polishing the substrates with sandpapers from grid 180 to 1000. Then, the surface roughness (Ra) is observed by a 3D optical profilometer (Alicona) to ensure that it is in the acceptable range for tribological tests using SRV testing machine. The testing balls are also obligatory to meet the surface finish 0.024 ± 0.005 μm Ra.

3. 2. PREPARATION OF THE COATINGS

The W-S-C coatings were prepared in 5 steps and will be elaborated in this section. The steps are illustrated by **Figure 3.1** as follows:

1. Sputter cleaning for WS_2 and C targets along with the cleaning of substrates.
2. Sputter cleaning of Cr and C targets with the cleaning process of substrates.
3. A Cr interlayer deposition
4. A deposition of Cr/W-S-C layer
5. A W-S-C layer deposition

Figure 3.1. Illustration of coating preparation

The coatings were deposited by magnetron sputtering facilitated by Instituto Pedro Nunes (IPN) utilizing 4 unbalanced magnetrons in a closed-field configuration and the instrument as shown in **Figure 3.2.** (a) and (b) respectively. The outer magnetic assembly of neighboring unbalanced magnetrons has opposite polarity, resulting in a closed magnetic ring. The closed magnetic field lines are in the vicinity of the substrates, entrapping the secondary electrons emitted by the target and thus ionizing the gas in the vicinity of the substrates. The enhanced plasma near the substrates can be used to sputter clean the substrates before deposition and/or bombard the growing film with Ar+ ions during deposition [42].

Figure 3.2. A sputtering magnetron instruments

An active inverted ionization gauge measures the ultimate vacuum pressure, which was less than 3 x 10^{-4} Pa prior to the deposition process, while a capacitance manometer measures the deposition pressure. The deposition took place in an Ar atmosphere. The rectangular planar targets, which are vertically aligned on the chamber walls. There were two graphite targets (99.99 percent purity) and a single TMD (WS_2, with 99.9 percent purity) to achieve a wide range of carbon contents. The graphite and TMD targets were bonded to a 4 mm thick copper backing plate with conductive silver filled epoxy. The targets were supplied by two different DC power outputs. First applied power are with 2 x 1400 W (as called sample W-S-C 1028) and 2 x 800 W (as called sample W-S-C 1016). This different output will define the power density of graphite (C) targets in order to achieve the different carbon content

Prior to deposition, the substrates and silicon wafers were attached to the surface of carrousel using conductive epoxy. A single rotation was applied to the substrates. The substrates were sputtered cleaned for 40 minutes before deposition. The targets were sputter cleaned simultaneously for 20 minutes, with a shutter covered the targets to avoid contamination during cleaning process. Targets C and WS_2 were cleaned first, followed by C and Cr. This cleaning procedure in pair provides plasma enhancement in the substrate region (via unbalanced magnetrons) and high ion current to be drawn on the substrates, resulting in cleaning efficiency and no additional heating is needed.

The selection of Cr as the interlayer was because Cr can form strong metallic bonds with steel substrates (DIN 100Cr6). The Cr interlayer was deposited for 10 minutes at a negative substrate bias voltage of 110 V. Following that, Cr/TMD-C gradient interlayer was gradually deposited by ramping down the power to the Cr target while by ramping up the power to the C and TMD targets to the deposition setpoint. In addition, the substrate bias was ramped down for TMD-C coating deposition. The gradient layer creates a more seamless transition in chemical composition. The details of the power output will be specified in **Tabel 3.1.**

Table 3.1. Parameters on deposition process

Steps	Conditions of targets	Conditions of substrates	Time
		Bias (V)	(min)
Cleaning WS2 and C targets	1000 W		20
Cleaning Cr and C targets	1000 W		20
Depositing a Cr interlayer	3 W/cm^2	110	10
Depositing a gradient Cr/W-S-C layer	Ramped down Cr and Ramped up WS2 and C	Ramped down to 0	10
Depositing a W-S-C layer (W-S-C 1028)	1400 W at the C targets and 1000 W at WS_2 target		60
Depositiing a W-S-C layer (W-S-C 1016)	800 W at the C targets and 1000 W at WS_2 target		60

3. 3. CHARACTERIZATION OF THE COATINGS

The coatings will follow some characterization processes to determine the properties of the coatings such as morphology, chemical composition, crystal structure, mechanical properties, adhesion and tribological properties using the methods as follows:

3.3.1. MORPHOLOGY

Scanning Electron Microscope (SEM, by Zeiss Merlin) was used to capture the images. The images were taken on cross-sectional surface and top surfaces of the freshly cleaved silicon wafer deposited with W-S-C coatings in different parameters mentioned in **Table 3.1.** Imaging was performed in an accelerating voltage of 2kV and with magnification 25 and 50 kx. This method is to observe the typical morphology on the coated surface and to measure the thickness of the coatings.

3.3.2. CHEMICAL COMPOSITION

Chemical composition was assessed using the same machine combined with a wavelength spectroscopy detector (WDS, by oxford instruments). The machine is supported with INCA software to analyze the composition. The analysis was performed with 15kV of accelerating voltage and the data were taken using INCA software.

3.3.3. CRYSTAL STRUCTURE

The crystal structure was analyzed by means of X-Ray Diffraction (XRD, by Malvern Panalytical X'Pert MRD). The experiments were carried out with parameters Co K_α (λ=1,79 Å) radiation (voltage of 40 kV and current of 45 mA). The experiment was set in incident angle of 3º, ranged from 10 to 90º, 3 seconds of time step, and 0.025º of step size. Then, the data was processed by origin and compared with the peaks with the International Center for Diffraction Data (ICDD) database.

3.3.4. MECHANICAL PROPERTIES

The mechanical properties that were observed are hardness and reduced modulus of elasticity measured by nano indenter and supported by a Berkovich type indenter. The coatings were tested in 16 points with an indentation load of 3 mN that reported better result in hardness and reduced modulus elasticity because the indented depth reaches~ 10% of coating depth. This indentation depth is to ensure that the properties of the substrate don't affect the testing

3.3.5. ADHESION PROPERTIES

The adhesion properties of the coatings were analyzed using scratch test (by Rtec universal tribometer machine shown in **Figure 3.3.**) and the indentation was using Rockwell C indentor with radius of 0.2 mm and progressive loads from 2 to 70 N. Then, the scratch tracks was captured by optical microscope (Alicona Infinite Focus^{TM} G4, see **Figure 3.4.**) to observe the locations of critical loads L_{C1}, L_{C2}, and L_{C3} with the help of ImageJ software. The parameters to determine critical loads were by finding the first appearance of cracks

(L_{C1}), the initiation of chipping and spallation at the borders of the scratch cracks (L_{C2}), and the fully delaminated coatings (L_{C3}).

Figure 3.3. Rtec universal tribometer machine equipped with optical microscope

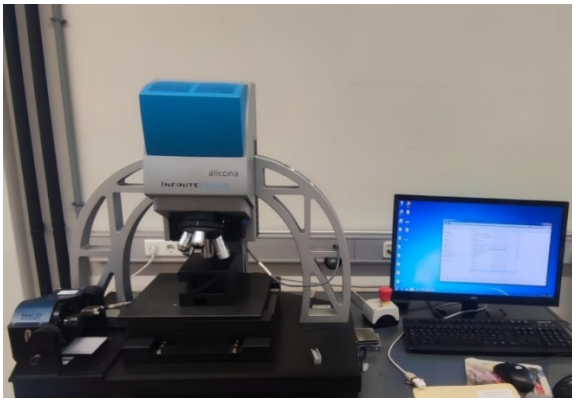

Figure 3.4. Alicona Infinite Focus™ G4

3.3.6. TRIBOLOGICAL PROPERTIES

A Linear-Oscilation (SRV) machine (facilitated by Instituto Pedro Nunes) was utilized to assess tribological properties of W-S-C coatings. The deposited disks were carefully prepared before the test following the preparatory procedures, see **Figure 3.5.** as follows:

1. Ultrasonically cleaning the deposited disks and testing balls in the bath heptane in a beaker measuring glass for about 15 minutes. It is to ensure that no oil contamination on the surface of coatings and testing balls
2. Rinsing the disks with flowing heptane first and then ethanol.
3. Applying testing parameters: normal load (50 N), frequency (50 Hz), stroke (s=1mm). The test procedure was following ASTM D-5707 for 2 hours (lubricated condition at 100 ºC and room temperature (RT)). The samples were tested for 10 minutes at dry condition at 100 ºC and a few minutes until the failure of coating was observed in dry condition at room temperature (RT). In lubricated condition, 0.05 ml of commercial engine oil (SAE 5W30) was added into the system. The detailed information on test parameters is explained in **Table 3.2.**

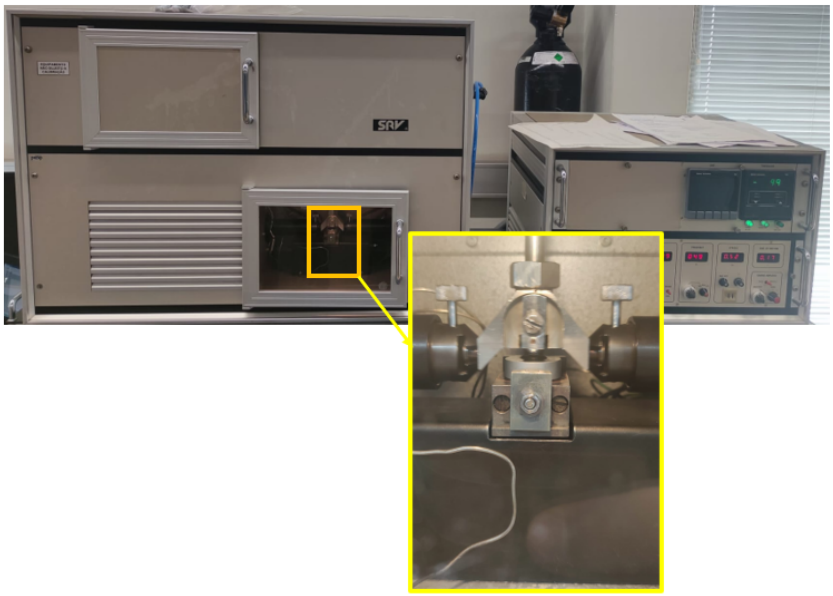

Figure 3.5. Preparation of the instruments

Table 3.2. Test parameters

Test parameters [units]	**Testing Conditions**			
	Lubricated		Dry	
	100 ºC	RT	100 ºC	RT
Load [N]	50			
Frequency [Hz]	50			

Stroke [mm]	1			
Speed [m/s]	0.1			
Tested specimens	100Cr6 vs 100Cr6	100Cr6 vs 100Cr6		
	100Cr6 vs W-S-C 1016	100Cr6 vs W-S-C 1016	100Cr6 vs W-S-C 1016	100Cr6 vs W-S-C 1016
	100Cr6 vs W-S-C 1028	100Cr6 vs W-S-C 1028	100Cr6 vs W-S-C 1028	100Cr6 vs W-S-C 1028

The coefficients of friction on each test were compared. Then, the topography images on the worn surfaces of each specimen were taken using 3D white light interferometer to observe the wear behaviour. These images were processed thoughtfully using Gwyddion to observe the topology and followed imaging procedures to obtain the representative areas of wear track using Origin Pro. Next, the obtained representative's area was assessed to gain the wear rate based on procedures mentioned in ASTM D7755-11 which was intended to analyze wear tracks by considering round edges to the sliding direction zone of the wear track shown in **Figure 3.6.** This method is perfectly matched with the testing parameters done in this experiment with stroke length (s) 1 mm, which standard is to assess wear track at high-frequency linear-oscilation with stroke length less than 2,5 mm. Some researchers postulated that the wear tracks on the flat specimens consist of 3 parts, the central/main part (A) and both small round edges (B). Some variables were taken into account in computing wear volume schematically illustrated in **Figure 3.6.** (c) and (d) as follows:

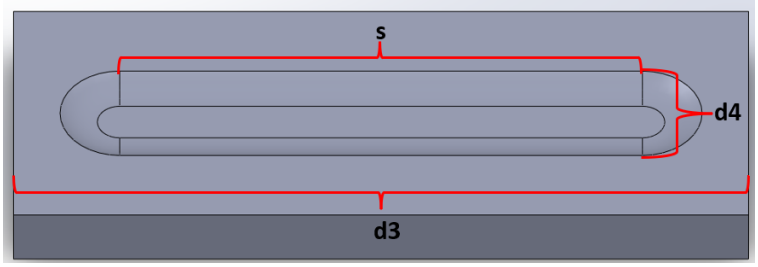

(a)

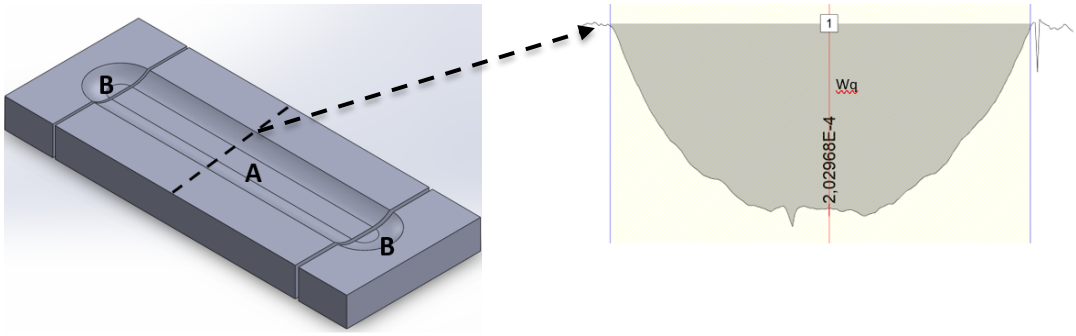

(b) (c)

Figure 3.6. Schematic illustration to calculate wear volume following ASTM D7755-11 standard. (a) Representative of sliding contact written with main identified parameters, (b) segmented representative parts, and (c) representative of cross-sectional wear (W_q).

The wear volume of each wear track by considering central part (A) and both rounded edges (B), then was computed with **Eq. 1** as follows:

$$W_{v,flat} = \frac{\pi\, x\, d_4^2\, (d_3 - s)^2}{64} * \frac{1}{\bar{R}} + s * W_q \qquad \textbf{Eq. 1 [43]}$$

It can be seen that d_3 is the total length of the wear trac in the sliding direction, d_4 is the width of the wear track, and $\bar{R}$ is the resulting radius of the cross-sectional shape of the wear track later after testing, see **Eq.2** below:

$$\bar{R} = \frac{d_4^2}{12\, x\, W_q} \qquad \textbf{Eq. 2 [43]}$$

The wear volume from the aforementioned steps above was then calculated to obtain wear rate by considering testing parameters in **Table 3.1.** Multiplying speed (V) and Time of sliding test (T) were used to get sliding distance (S) shown in **Eq. 3.** Finally, the wear rate was obtained by dividing the wear volume ($W_{v,flat}$) with the multiplication of load (F) and sliding distance (S) seen in **Eq. 4.**

$$S = V * T \qquad \textbf{Eq. 3}$$

$$Speciic\ wear\ rate = \frac{(W_{v,flat})}{F * S} \qquad \textbf{Eq. 4}$$

CHAPTER 4

4. RESULTS DISCUSSION

In this part, W-S-C coatings were depsosited and characterized in order to study its morphology and composition, structure, mechanical properties, adhesion and tribological properties. Previous studies mainly focused on the performance of self-lubricating TMD coatings on dry contact. Thus, this study will be used to improve future development of self-lubricating TMD coatings in the lubricated condition. The results of this study will be further described below:

4.1. MORPHOLOGY

The morphology features were captured and analyzed using scanning electron microscope (SEM by Zeiss Merlin) on the top-view surfaces of each coating and cross-sectional surfaces of coating to better understand the thickness and the morphology of the coating layers (Cr interlayer, gradient Cr/W-S-C layer and W-S-C layer) as the result of different deposition parameters. On top-view surfaces, cauliflower-like structures can be seen in both coatings, see **Figure 4.1.** (b) and (d).

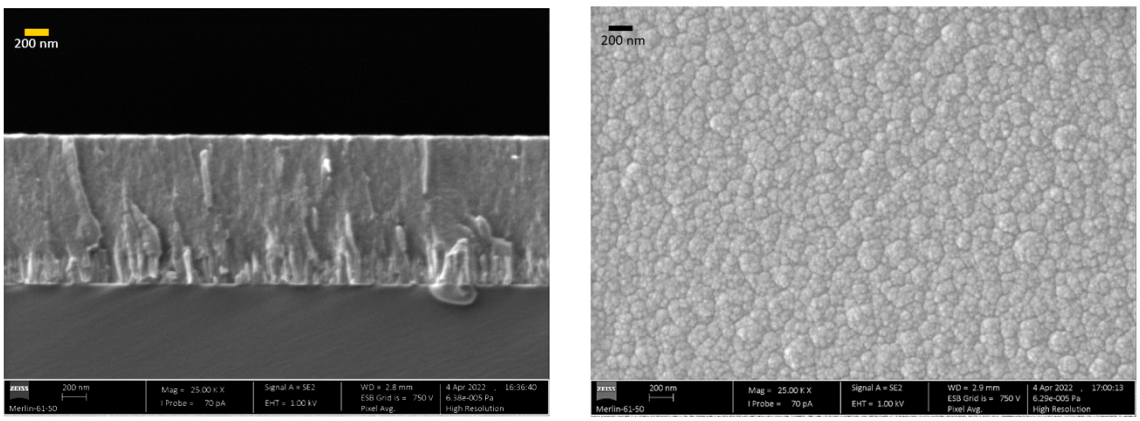

(a) (b)

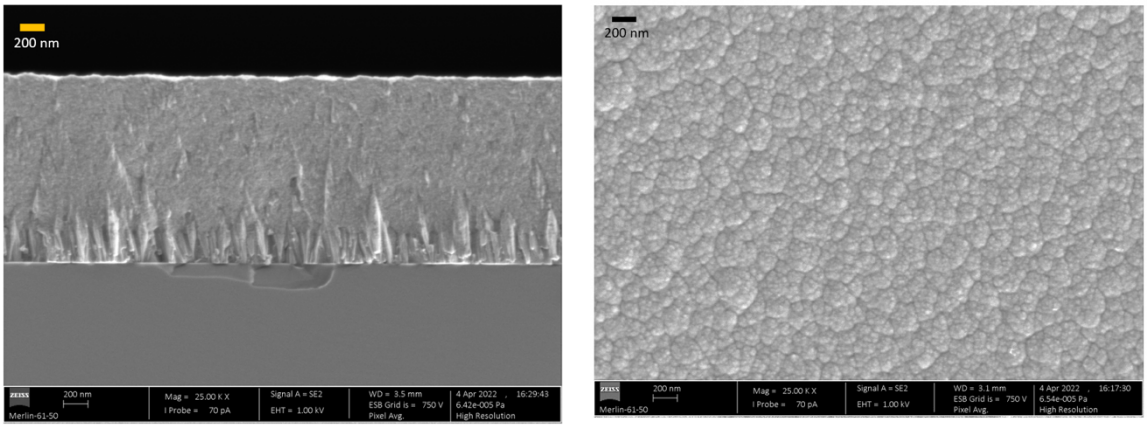

(c) (d)

Figure 4.1. Morphology features of W-S-C coatings (a) W-S-C 1016 top view, (b) W-S-C 1016 cross-sectional view, (c) W-S-C 1028 top view, and (d) W-S-C cross-sectional view.

It is commonly found and supported by some researchers in the deposited films by magnetron sputtering because it is affected by atomic shadowing effect. With the same maginification, there is a slight difference on the size of cauliflower-like structure. W-S-C 1028 structures created bigger crowns which are densed and smoother than W-S-C 1016. It is the result of the difference supplied power. Some researchers [30,36 and 43] confirmed in their research work that higher supplied power will improve smoothening effect on the surfaces of the coating. Higher target voltage will enhance the generation of backscattered Ar neutral. The smoothening surface might be caused by the increased bombardment of the growing film with the reflected Ar neutrals because the increase of backscattered Ar neutral in W-S-C is higher. The increased bombardment of growing film is proportional with the adatom mobiity leading to the reduction of atomic shadowing effect [44]. The cross-sectional images, see **Figure 4.1.** (a) and (c) show columnar growth in both coatings. It is obvious that columnar features on W-S-C 1016 grows longer and almost reachs top surface than columnar features on W-S-C 1028 which can be found around Cr interlayer and or Cr/W-S-C gradient layer. The structure of W-S-C 1028 appears more compact between Cr/W-S-C gradient layer and W-S-C layer in comparison with W-S-C 1016 coating. It is supported by Vuchkov et al.'s finding [34,43] that it is due to target powers. In addition, the thickness of deposited W-S-C coatings typically vary from 1.2 to 1.5 μm and this research work followed the same trend in which the values of thickness are of 1.3 μm for W-S-C 1016 and of 1.5 μm for W-

S-C 1028 coatings. In both cases, it is quite difficult to define the interface between Cr/W-S-C gradient layer and W-S-C layer, but it can be seen the transition of the extended columnar structure slowly disappears. In addition, Vuchkov et al. [36] and Yakub et al. [30] mentioned that this smoothening effect is related with the chemical composition of the coatings. The chemical composition of coatings will be explained further.

4.2. CHEMICAL COMPOSITION

The elemental composition of the deposited W-S-C coatings is presented in **Table 4.1.** by means of Wavelength-Dispersive X-Ray Spectroscopy (WDS). The results shows the sum of W,S,C and O at.%. The increase of powers on carbon targets affected the C contents on the coatings. The higher applied power on C targets resulted in the higher content of C in the coating. W-S-C 1028 reached about 45.6 at. % of C content. On the other hand, W-S-C 1016 with lower power on C target resulted in 35.5 at. % of C content. The oxygen content existed on the coatings is likely from the contamination on the target and residual oxygen in the chamber.

Table 4.1. Chemical composition and S/W ration of coatings

Coatings	**Chemical composition at. %**				**S/W ratio**	**Thickness (µm)**
	W	S	C	O		
W-S-C 1016	25.1± 0,1	36.1± 0,2	35.5± 0.2	2.8± 0.1	1.4	1.3
W-S-C 1028	21.1	30.1± 0.1	45.6± 0.1	2.8± 0.1	1.4	1.5

The sulphur to tungsten ratio (S/W) in the deposited films is essential since it affects the tribological performance [45]. Vuchkov et al. [43] presented the values of S/W ratio for the coatings deposited by magnetron sputtering reach between 1 and 1.7. In both coatings, the values of S/W ratios are similar of 1.4 for both coatings. These values are fall into categories presented by Vuchkov et al. [36]. In his research, he opined that the S/W ratio is the result of scattering behaviors that the sputtered species (C,S and W) bring its own behaviours. Due to the light weight of C and S atoms, they tend to collide with the Ar gas in the chamber leading to rich atoms of C and S causing the reduction of energetic Ar neutrals

because of the increase of collision in the system. W-S-C 1028 contains higher C due to higher applied power on the C targets. W-S-C 1028 applied 1400 W of power on each C target and the power supply for WS_2 target is of 1000 W. As a result, higher content of carbon on the deposited coatings was found in this sample in comparison with sample of W-S-C 1016 which the applied power on each C target is lower. The increase of carbon content is likely caused by the lower sputtering yield of carbon. [43]

4.3. CRYSTAL STRUCTURE

The deposited films of W-S-C coatings were characterized by X-Ray Diffraction method to find the patterns by analyzing the visible peaks of WS_2. The result is shown in **Figure 4.2.**

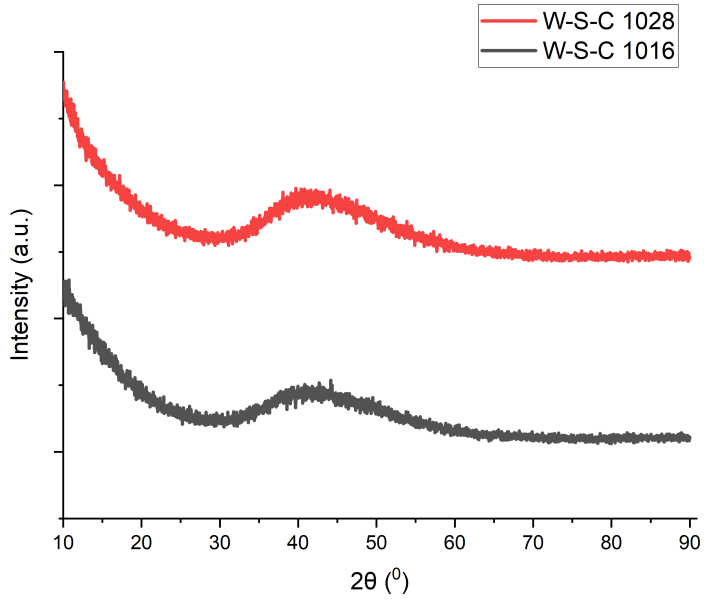

Figure 4.2. XRD diffractogram of deposited W-S-C coatings

The result of XRD characterization showed that there was a identified broad peak starting from 2θ of 30º to 50º indicating the presence of amorphous crystal structure. In some research, peaks such as basal oriented crystals and Cr peak were observed during XRD examination but in this research work, those peaks were not detected.

In Vuchkov et al. [42] research on W-S-C coatings, he found that basal oriented crystal were clearly detected at~ 10-14º of 2θ as the small reflection of WS_2 (002) almost parallel with the substrate. On the other hand, on this research, basal plane was not detected around the presented values of 2θ. In addition, the presence of broad peak starts at ~33º of

2θ indicating peaks of family WS_2 which is also supported by Mutapof et al. [46] in their experiment mentioning that the asymmetric peak is elongated on right with the visible peak ranging from 30º to 45º of 2θ [46,47]. Cr peak cannot be detected that is supposedly found around 52º of 2θ based on ICCD card no. 01-085-1335 and other families of WS_2 are difficult to be detected since there are many broaden peaks in the regions of 2θ ranging from ~33.8º to 46.3º referring to ICDD card no. 00-009-0237. The broaden peak of W-S-C 1028 is likely stretched longer than of W-S-C 1016. It is about~35º to 55º of 2θ.

4.4. MECHANICAL PROPERTIES

The mechanical properties were focused in the analysis of hardness and reduced modulus elasticity. The x-axis shows the applied load during the indentation and y-axis shows the values of hardness. The hardness values were ~5.7 GPa and ~6.5 GPa for W-S-C 1016 coating and W-S-C 1028 coating respectively. The reduced modulus elasticity showed no significant change of around 97 GPa for both coatings. The increase of hardness is projected in the increase of carbon content which is related to higher power applied to the carbon targets. In Vuchkov research work [42], he deposited a W-S-C coating by magnetron sputtering with different supplied power on the targets, the increase of power on the targets, the higher content of targets he obtained. The trend shows that the increase of carbon content up to 45.6% is correlated to the increase of hardness. The hardness values of W-S-C 1028 increased~13% from the values of W-S-C 1016 with 35,5% carbon content.

Hardness of the coatings is commonly found because of the reduced S/W ratio but both coatings have the same S/W ratio of 1.4. The ratio of S/W signifies that more tungsten is available for the formation of hard tungsten carbide inclusions. The increase of tungsten carbide phases is likely causing the increase of hardness. In the case of equal number of carbides, the hardness is correlated by the presence of a-C phase [42]. Unfortunately, it doesn't present in the XRD characterization. It is likely the size is very small or in the amorphous phase in term of a-C matrix [49]. Higher S/W ratio signifies the higher presence of WS_2. It explains lower hardness in W-S-C 1016 coatings. Moreover, W-S-C 1028 was supplied with higher power on the C targets to increase the bombardment level the growing film with Ar neutrals. The bombardment increased the densification of the morphology because of the increased adatom mobility [44]. The denser and more compact morphology indicates higher hardness [48,50]. This trend can be seen in the load indentation of 3 mN.

Polcar et al. [50] explained that the increase of hardness based on the carbon content reaches its maximum hardness at~40 at. % C. The hardness started to decrease in an increase of carbon content more than~40 at. %. In addition, reduced modulus of elasticity is in a similar trend with the increase of hardness [50]. Adhesion is necessary since the coating materials and substrate materials have different properties. Therefore, the adhesion is being the next topic to be discussed.

4.5. ADHESION PROPERTIES

Adhesion of the W-S-C films to the substrate was characterized by observing the scratch scars through optical microscopy. The results are presented in **Figure 4.3.** Failure mechanism of coating was observed in the term of critical load values and where the points are located. L_{c1} is identified in load where the start of crack formation on the edges of the scratch scars, L_{c2} is ascociated with the load at which the chipping process has started on the border of the scratch scars, and L_{c3} load is correlated with the load where the spallation or delamination of the films occurs [51] which is related to the exposure of the interlayer of the substrate. W-S-C coating deteriorated in a lower applied load. The critical load 1 (L_{c1}) and 2 (L_{c2}) were found at 11 N and at 26 N respectively. The values of L_{c1} and L_{c2} of W-S-C 1016 coatings are slightly higher at 12 N and 29 N, see **Table 4.2.**

The coating with worst adhesion (W-S-C 1016) shows delamination at 58,61 N which quite remarkable in comparison with Vuchkov et al. research [42]. With the amount of carbon content (47, 6 at.%), the critical load 3 (L_{c3}) happened in smaller L_{c3} of 37 N. It indicates the improved adhesion in smaller content of carbon. Surprisingly, W-S-C 1028 coating doesn't show any delamination of the films. The surface of sratch scar is almost similar all over the surface indicating the better adhesion which can be the presence of Cr as the interlayer and or more compact morphology leading to more resistant in cracking. The hardness properties affect the toughness of the coatings. Moreover, Polcar et al. [50] deposited W-S-C coatings with carbon content of 29, 40, 51 and 64 at. %. They reported the decrease hardness in the coating with carbon content above 50 at. %. As a result, it increases the brittleness [50]. Limited research observes the exact amount of carbon content in the range between 40 at. % and 50 at. % . Based on Polcar et al. W-S-C coating consisted of carbon content between 40 at. % and 50 at. % experienced unique feature by dropping its hardness and lower brittleness [50].

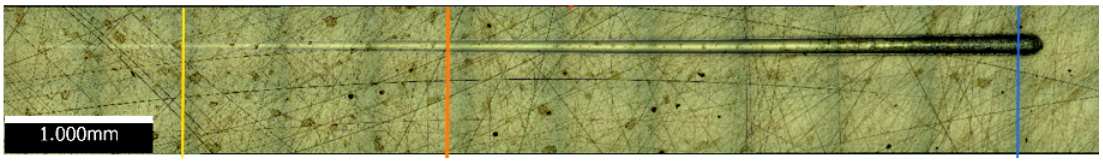

(a) W-S-C 1016

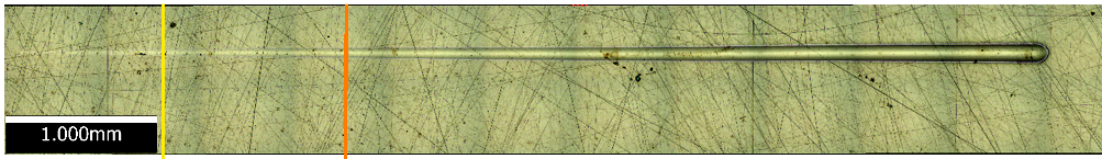

(b) W-S-C 1028

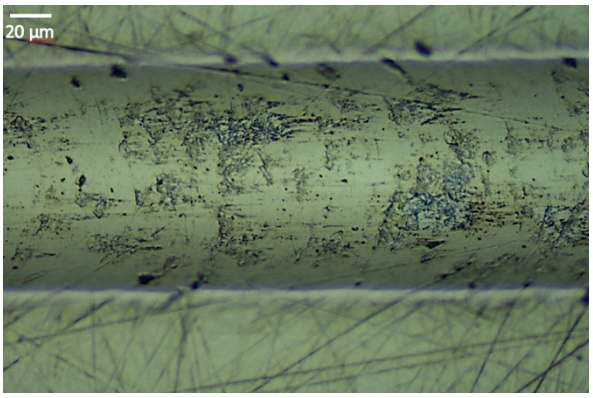

(c) L_{c2} W-S-C 1016

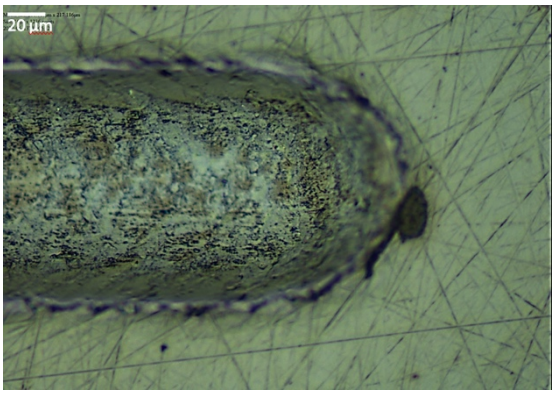

(d) L_{c3} W-S-C 1016

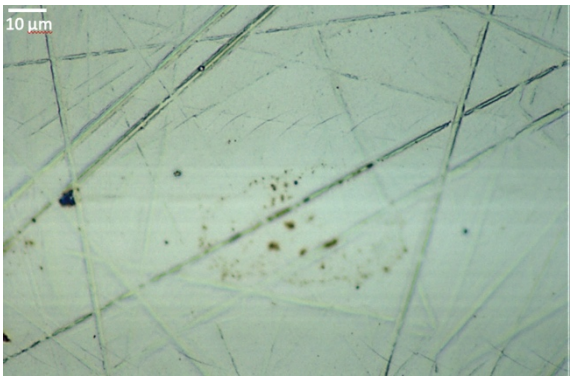

(e) L_{c1} W-S-C 1028

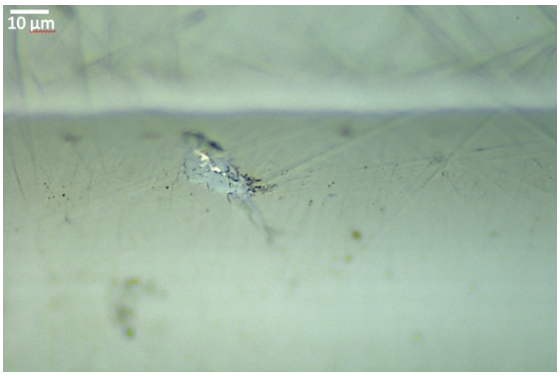

(f) L_{c2} W-S-C 1028

Figure 4.3. Scratch scars on optical microscope (a) W-S-C 1016, (b) W-S-C 1028, (c) detailed L_{c2} on W-S-C 1016, (d) detail L_{c3} on W-S-C 1028, (e) detail L_{c1} on W-S-C 1028, and (f) detail L_{c2} on W-S-C 1028

Table 4.2. Mechanical properties and adhesion

Coating	Hardness (GPa)	Reduced modulus of elasticity (GPa)	Critical Load L_{c1} (N)	Crticial Load L_{c2} (N)	Critical Load L_{c3} (N)
W-S-C 1016	6.8 ± 1.0	97.0± 12.8	11.7 ± 2.6	29.0± 1.3	58.6
W-S-C 1028	7.1 ± 0.7	97,0± 6.8	11,0± 1.5	25,5± 4.0	

4.6. TRIBOLOGICAL PROPERTIES

Tribological properties of the coatings will be investigated by the analysis of Coefficient of Friction (CoF) and wear track in the lubricated and dry conditions. In each condition, the performance of coatings in the higher temperature was also observed to understand the effect of temperature in the CoF and specific wear rate in lubricated and dry conditions.

4.6.1. COEFFICIENT OF FRICTION (COF) ANALYSIS

4.6.1.1. COF analysis in lubricated condition

The coefficient of friction vs number of cycles in the lubricated condition is shown in **Figure 4.4.** (a) at 100 ºC and (b) at room temperature (RT). In this graph, it can also be seen the value of COF for uncoated substrates. At 100 ºC, the CoF of uncoated substrates reaching ~ 0.17 is higher in comparison with the coated substrates. It proved that W-S-C coating improves the tribological properties by lowering the CoF. Noises were observed in both coatings. It is likely due to the measuring interference from the delaminated or spallation of coating layers.

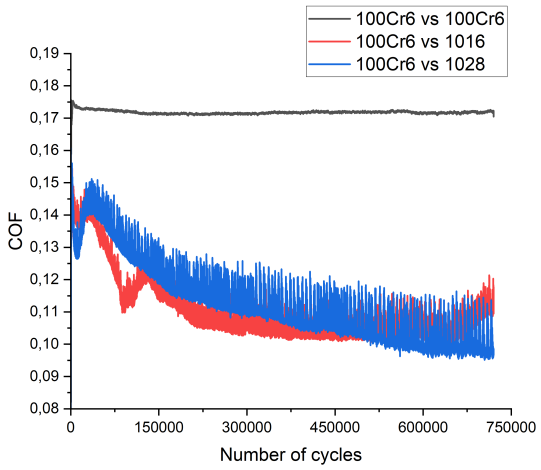

(a) At 100 ºC

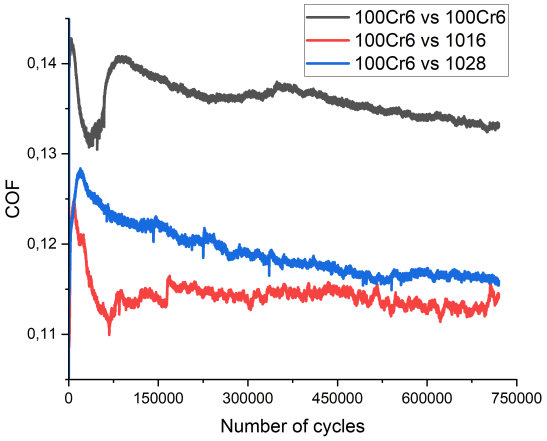

(b) At room temperature (RT)

Figure 4.4. COF in lubricated condition (a) at 100 ºC and (b) at room temperature (RT)

Initially there is not much different in the values of CoF for W-S-C 1016 and 1028. The values of CoF in the beginning of the test were~0.14. Then, running-in stage was taken place until the CoF dropped down. CoF of W-S-C 1028 was reported higher than W-S-C 1016 until the number of cycles reached about 450000. It continuously dropping to~0.10. On the other hand, W-S-C 1016 increased starting from the same number of cycles and reached to~0.12 in the end of the testing period.

It is importance to remember that W-S-C 1016 contains lower carbon and higher tungsten disulphide which is softer and easily to break in comparison with W-S-C 1028 coating. The WS_s platelets inside the coating reoriented in parallel direction with sliding contact and form WS_2 tribolfilm during tribological contact. The CoF of W-S-C 1060 remained lower than W-S-C 1028 until number of cycles reaching 450000. Then, it went up

to surpass COF of W-S-C 1028 which is likely from the presence of alloy elements close to the interface of tungsten disulphide tribofilm. This coating has lower amount of WS_2 in the coating. Once it formed tribofilm during tribological contact, the tungsten disulphide tribofilm was depleted. Thus, the increase of CoF is observed in the experiment. The interference of alloy elements in testing W-S-C at 100 ^{0}C distracted the formation of tribofilm. Thus, it increased the interfacial shear strength and the friction [27]. In addition, the system was in a lubricated sliding contact. The test might form boundary lubricated sliding contact. The lubricant used was SAE 5W30 contains a small amount of sulphur. A transfer of tungsten and or sulphur elements to the interface might react to sulphur from the lubricant formed easy-shear tungsten disulphide tribofilm layer. The reaction between tungsten element from the coating and sulphur element from the lubricant might happen in the condition which there is abundant amount of unbonded W in the coating film.

4.6.1.2. COF analysis in dry condition

In addition, in dry condition, the value of CoF is shown in **Figure 4.5.** W-S-C coatings showed quite low CoF of 0.015 at 100 ºC. It is expected to happen due to lack of humidity in the contact system and high temperature facilitate the formation of crystalline slipping of weakly bonded basal oriented structure to decrease the coefficient of friction [50]. The coating with higher carbon content showed the decrease of C0F after 15000 number of cycle and stayed constant until it reached 55000 number of cycles. Then, it showed a significant rise of CoF until the end of test. The test was limited to 10 minutes continuously running test which is equal to 60000 number of cycles due to it is operated in dry condition. Vuchkov in his research, he reported the failure of W-S-C coating happened at~ 10000 for higher load (35N) [42]. This experiment was performed at 50N applied load. It is the reason why the test was carried by limiting the testing time.

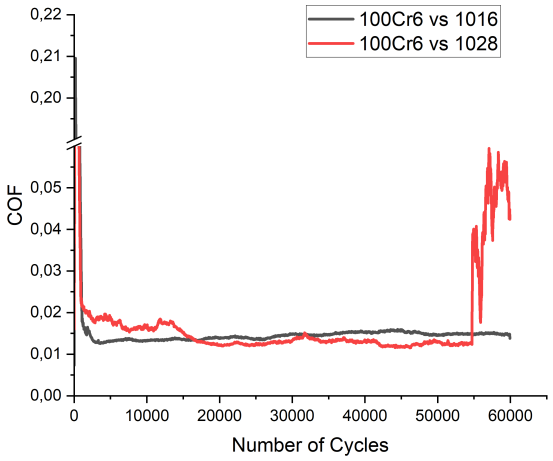

(a) At at 100 ºC

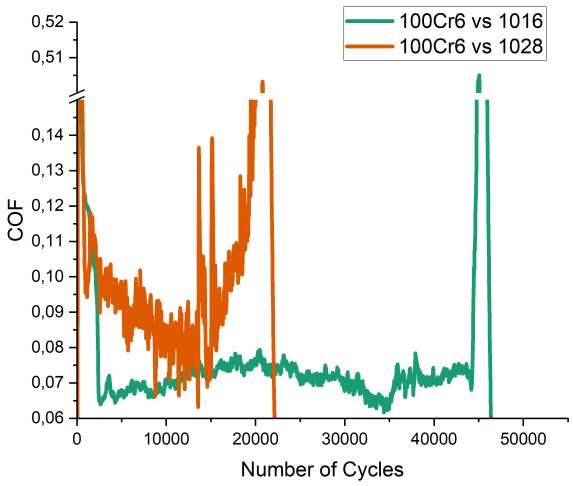

(b) At room temperature (RT)

Figure 4.5. CoF in dry condition (a) at 100 ºC and (b) at room temperature (RT)

In addition, in dry condition, the W-S-C coatings showed quite low CoF of 0.12-0.16 at 100 ºC. It is expected to happen due to lack of humidity in the contact system and high temperature facilitate the formation of crystalline slipping of weakly bonded basal planes to decrease the coefficient of friction [50]. The coating with higher carbon content showed the decrease of CoF after 15000 number of cycle and stayed constant until it reached 55000 number of cycles. Then, it showed a significant rise of CoF until the end of test. The test was intended reaching about 60000 number of cycles due to it is operated in dry condition. Vuchkov in his research, he reported the failure of W-S-C coating happened at~ 10000 for higher load (35N) [42]. In this experiment, it was tested at 50N of load which is

higher, and it was expected to fail in short period of number of cycles. Thus, the test was set in 60000 number of cycles. If the test was running continuously, there would be a failure in the coating layer in a short time. It indicates that higher carbon content and higher hardness coating signified the easily deterioration of the coating leading to the increase of wear rate.

On the other hand, at the room temperature, the coatings failed in lower number of cycles. The values of CoF fluctuated in was about 0.07 for W-S-C 1016 and 0.12 for W-S-C 1028. In this condition, it followed the same pattern of failure. W-S-C coating failed in low number of cycles of 20000, but it was about 45000 of number of cycles for W-S-C 1016. The high CoF was projected in lower temperature since the humidity is higher. Vuchkov reported that CoF of W-S-C coating at room temperature was around 0.14. This value is comparable to the value from this experiment. He also pointed out that the rise of COF affected the specific wear rate or wear as a process causing energy dissipation resulting in the increase of friction that will be discussed further.

4.6.2. SPECIFIC WEAR RATE ANALYSIS

4.6.2.1. Specific wear rate analysis in lubricated condition

The analysis of specific wear rate in lubricated contact is shown in **Figure 4.6** and **Table 4.3.** In the contacting surfaces, initially, the coating is worn off and gets aligned with the sliding direction forming WS_2 tribofilm leading to the reduction of COF. W-S-C coatings consist of easy-shear deposited layers which can be depleted to form tribofilm. The formation of tribofilm is related to the wear rate of each coating to fulfil its role in the reduction of CoF. The hypothesis was that the easily deteriorated coatings would form much tribofilm and reduce the CoF. It is the reason why the COF values were low. In this experiment, the specific wear rate analysis was observed the effect of testing temperatures. The specific wear rate of W-S-C 1016 were reported higher than specific wear rate of W-S-C 1028 that is expected to happen by considering the nature of WS_2. WS_2 layer has weaker bond and is easily torn apart. It goes the same trend in this experiment where W-S-C 1016 contains richer tungsten and sulphur leading to more porous structure in comparison with W-S-C 1028 indicating compact and denser morphology structure. The wear volume also

supported this statement. The specific wear rates are 1.3 x 10^{-8} mm^3/Nm (100 ºC) and 8.6 x 10^{-9} mm^3/Nm (RT).

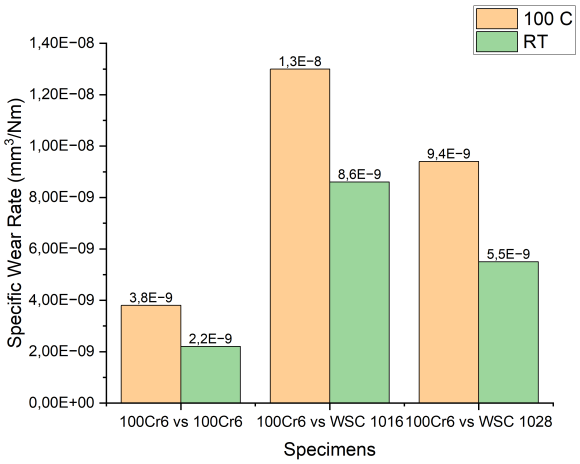

Figure 4.6. Specific wear rate at lubricated Specific wear rate in lubricated condition

Table 4.3. Specific wear rate and wear volume in lubricated condition

Properties	**100 ° C**		**RT**	
	100Cr6 vs 1016	100Cr6 vs 1028	100Cr6 vs 1016	100Cr6 vs 1028
Wear volume of wear scar	4.6E-04	3.4E-04	3.1E-04	2.0E-04
Specific wear rate	1.3E-08	9.4E-09	8.6E-09	5.5E-09

In both temperature testing, test at room temperature showed lower specific wear rate. The transfer of tungsten and sulphur elements from the coatings was facilitated by the presence of lubricant containing sulphur-based additives. Higher content of tribofilm in the system resulted in lower CoF reported in the previous analysis where W-S-C 1016 has lower CoF value. In this experiment, the coatings itself already consist of tungsten and sulphur elements where the lubricant containing sulphur-based additive doesn't interfere the formation of WS_2 tribofilm. But to ensure the formation of triboactive film, further study in the tribochemistry and experiments in other lubricants containing various content of sulphur is expected in the future study.

4.6.2.2. Specific wear rate analysis in dry condition

The analysis of specific wear rate in dry contact is shown in **Figure 4.7** and **Table 4.4.** On the contrary with the performance of coating in lubricated condition, the

performance of the coatings in dry conditions showed high specific wear rate in both testing temperatures. W-S-C 1028 coatings experienced the highest specific wear rate about 1.0 x 10^{-7} mm^3/Nm and 1.4 x 10^{-7} mm^3/Nm for testing temperature at 100 ºC and RT respectively. The coating with higher carbon content showed a high worn volume. In the room temperature, the tribological behavior might be determined by the development of a tribofilm between the surfaces in the contact or and by the transfer of the self-lubricant material to the steel counter ball.

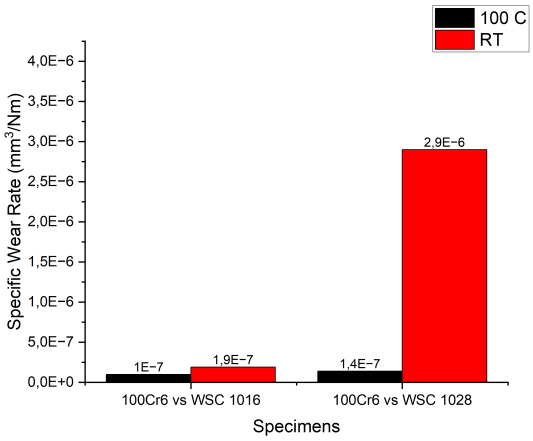

Figure 4.7. Specific wear rate in dry condition

Table 4.4. Specific wear rate and wear volume in dry condition

Properties	**100 ºC**		**RT**	
	100Cr6 vs 1016	100Cr6 vs 1028	100Cr6 vs 1016	100Cr6 vs 1028
Cross sectional wear volume (mm^3)	3.1E-04	4.3E-04	4.5E-04	3.2E-03
Specific wear rate (mm^3/Nm)	1.0E-07	1.4E-07	1.9E-07	2.9E-06

Let us go back at **Figure 4.5.** (b). For the specimen W-S-C 1028, the initial CoF values were high during running-in and dropped down significantly. It is likely that the tribofilm layer were already created, then the constant state of wear rate was achieved. It is the reason why the specific wear rate of 1.9 x 10^{-7} mm^3/Nm in 100 ºC in were in the comparable values with the specific wear rate W-S-C 1016 in both testing temperatures. On the other hand, it soared up in the RT testing condition reaching 2.9 x 10^{-6} mm^3/Nm which is ~21 times higher than in 100 ºC testing condition. In this high-carbon content coating, limited tungsten disulphide presents, therefore, the system is lack of raw material to form

tribofilm in the sliding contact. As a result, the initial friction force is considerably high leading to severe damage to the coating surface [50].

CHAPTER 5

5. CONCLUSION

Considering series of test to determine the properties of W-S-C coatings, this research work can fulfil the objectives and summed up as follows:

1. The applied power on C targets affects the chemical composition of carbon on the coatings. Higher power supplied increases the carbon content on the coatings
2. The increase of testing temperature shows the alteration of CoF and specific wear rate. In lubricated conditions, at 100 ºC, the CoF of specimens coated with W-S-C is lower in comparison with the uncoated specimens. Spiky data were detected during the measurements due to the interference from the delaminated coating layers. The specific wear rate at 100 ºC is higher because of the transfer of tungsten and sulphur elements from the coatings to facilitate formation tribofilm. The existence of sulphur-based oil lubricant doesn't interfere the formation of WS_2 tribofilm. To compare, in dry condition, at 100 ºC, the low CoF is expected due to the lack of humidity in the contact system and high temperature improve the formation of crystalline slipping of weakly bonded basal planes to decrease CoF. In addition, the specific wear rate shows lower than specimens tested at room temperature where the coating layers are easily delaminated. As a result, the specific wear rate rises up significantly. Thus, the effect of temperature plays a role in the formation of tribofilm to improve the tribological properties of W-S-C coatings.
3. The additional oil lubricant was intended to reveal the existence of tribofilm affecting coefficient of friction and specific wear rate. In lubricated condition, higher CoF and low specific wear rate signified the transfer of tungsten and or sulphur elements to the counter ball with the help of liquid lubricant containing sulphur-based additive. The presence of liquid lubricant didn't act antagonistically since it already contains additive with sulphur. As a result, the specific wear rate is low and durable in high number of cycles, even though it shows high coefficient of friction. In comparison with testing in dry condition, the test resulted low coefficient of friction and high specific wear rate. Moreover, the coatings were failed in low number of cycles indicating low durability. This solid lubricant still cannot diminish the function of liquid lubricant.

CHAPTER 6

6. FUTURE WORK

The development of WS alloyed with carbon coating still need improvement in term of performance. Thus, some ways can be carried out to clarify some doubts from this research projects. They are:

1. Deposition with supplied powers on the targets C to obtain C content in the range of 40-50%. Polcar T et al. reported that starting from 50% of C content, the properties of coatings decrease [40].
2. Deep characterization on the amorphous nanocrystalline structure by using TEM (Transmision Electron Microscopy)
3. Tribological test on higher temperature (200, 300 or 400 ºC) in lubricated and dry contacts.
4. Different types and contents of lubricants used in the tribologiºcal test to fully understand the transfer of the coatings elements.
5. Deeper study in tribochemistry of the lubricated contacts.

CHAPTER 7

7. REFERENCES

[1] Stachowiak, & Batchelor, A. W. (2001). Engineering tribology (Second edition.). Butterworth-Heinemann.

[2] Voevodin, A.A., Muratore, C., & Aouadi, S.M. (2014). Hard coatings with high temperature adaptive lubrication and contact thermal management: review. *Surface & Coatings Technology, 257*, 247-265.

[3] Yaqub, T.B., Hebbar Kannur, K., Vuchkov, T., Pupier, C., Héau, C., & Cavaleiro, A. (2020). Molybdenum diselenide coatings as universal dry lubricants for terrestrial and aerospace applications. *Materials Letters, 275*, 128035.

[4] Pimentel, J.V., Polcar, T., Evaristo, M., & Cavaleiro, A. (2012). Examination of the tribolayer formation of a self-lubricant W–S–C sputtered coating. *Tribology International, 47*, 188-193.

[5] Polcar, T., & Cavaleiro, A. (2011). Review on self-lubricant transition metal dichalcogenide nanocomposite coatings alloyed with carbon. *Surface & Coatings Technology, 206*, 686-695.

[6] Choi, W., Choudhary, N., Han, G.H., Park, J., Akinwande, D., & Lee, Y.H. (2017). Recent development of two-dimensional transition metal dichalcogenides and their applications. *Materials Today, 20*, 116-130.

[7] Pimentel, J.V., Danek, M., Polcar, T., & Cavaleiro, A. (2014). Effect of rough surface patterning on the tribology of W–S–C–Cr self-lubricant coatings. *Tribology International, 69*, 77-83.

[8] Bowden, & Tabor, D. (1942). Mechanism of Metallic Friction. Nature (London), 150(3798), 197–199.

[9] Rapuc, A., Wang, H., & Polcar, T. (2021). Nanotribology of transition metal dichalcogenide flakes deposited by chemical vapour deposition: The influence of chemical composition and sliding speed on nanoscale friction of monolayers. *Applied Surface Science, 556*, 149762.

[10] Fan, X., & Wang, L. (2014). Highly conductive ionic liquids toward high-performance space-lubricating greases. *ACS applied materials & interfaces, 6 16*, 14660-71 .

[11] Rapuc, A., Simonović, K., Huminiuc, T., Cavaleiro, A., & Polcar, T. (2020). Nanotribological Investigation of Sliding Properties of Transition Metal Dichalcogenide Thin Film Coatings. *ACS applied materials & interfaces*.

[12] Tomala, A., Vengudusamy, B., Rodríguez Ripoll, M., Naveira Suarez, A., Remškar, M., & Rosentsveig, R. (2015). Interaction Between Selected MoS2 Nanoparticles and ZDDP Tribofilms. *Tribology Letters, 59*, 1-18.

[13] Roberts, E.W. (1990). Thin solid lubricant films in space. *Tribology International, 23*, 95-104.

[14] Voevodin, A.A., O'Neill, J.P., & Zabinski, J.S. (1999). Nanocomposite tribological coatings for aerospace applications. *Surface & Coatings Technology, 116*, 36-45.

[15] Zhou, F., Liang, Y., & Liu, W. (2009). Ionic liquid lubricants: designed chemistry for engineering applications. *Chemical Society reviews, 38 9*, 2590-9 .

[16] Palacio, M.L., & Bhushan, B. (2010). A Review of Ionic Liquids for Green Molecular Lubrication in Nanotechnology. *Tribology Letters, 40*, 247-268.

[17] Kawada, S., Watanabe, S., Kondo, Y., Tsuboi, R., & Sasaki, S. (2014). Tribochemical Reactions of Ionic Liquids Under Vacuum Conditions. *Tribology Letters, 54*, 309-315.

[18] Scharf, T.W., & Prasad, S.V. (2012). Solid lubricants: a review. *Journal of Materials Science, 48*, 511-531.

[19] Polcar, T., & Cavaleiro, A. (2011). Self-adaptive low friction coatings based on transition metal dichalcogenides. *Thin Solid Films, 519*, 4037-4044.

[20] Xu, S., Sun, J., Weng, L., Hua, Y., Liu, W., Neville, A., Hu, M., & Gao, X. (2018). In-situ friction and wear responses of WS2 films to space environment: Vacuum and atomic oxygen. *Applied Surface Science*.

[21] Xu, S., Hu, M., Sun, J., Weng, L., Liu, W., & Gao, X. (2018). A simple strategy to tailor the microstructure and wear-resistance of sputtered WS2 films. *Materials Letters, 216*, 179-181.

[22] Scharf, T.W., Rajendran, A., Banerjee, R., & Sequeda, F.O. (2009). Growth, structure and friction behavior of titanium doped tungsten disulphide (Ti-WS2) nanocomposite thin films. *Thin Solid Films, 517*, 5666-5675

[23] Nossa, A., & Cavaleiro, A. (2001). The influence of the addition of C and N on the wear behaviour of W–S–C/N coatings. *Surface & Coatings Technology, 142*, 984-991.

[24] Hirvonen, J., Koskinen, J., Jervis, J.R., & Nastasi, M. (1996). Present progress in the development of low friction coatings. *Surface & Coatings Technology, 80*, 139-150.

[25] Zekonyte, J., & Polcar, T. (2015). Friction Force Microscopy Analysis of Self-Adaptive W-S-C Coatings: Nanoscale Friction and Wear. *ACS applied materials & interfaces, 7 38*, 21056-64 .

[26] Hebbar Kannur, K., Yaqub, T.B., Huminiuc, T., Polcar, T., Pupier, C., Héau, C., & Cavaleiro, A. (2020). Synthesis and structural properties of Mo-S-N sputtered coatings. *Applied Surface Science, 527*, 146790.

[27] Gustavsson, F., Jacobson, S., Cavaleiro, A., & Polcar, T. (2013). Ultra-low friction W–S–N solid lubricant coating. *Surface & Coatings Technology, 232*, 541-548.

[28] Isaeva, L., Sundberg, J., Mukherjee, S., Pelliccione, C.J., Lindblad, A., Segre, C.U., Jansson, U., Sarma, D.D., Eriksson, O., & Kádas, K. (2015). Amorphous W–S–N thin films: The atomic structure behind ultra-low friction. *Acta Materialia, 82*, 84-93.

[29] Yaqub, T.B., Vuchkov, T., Evaristo, M., & Cavaleiro, A. (2019). DCMS Mo-Se-C solid lubricant coatings – Synthesis, structural, mechanical and tribological property investigation. *Surface and Coatings Technology*.

[30] Yaqub, T.B., Vuchkov, T., Sanguino, P., Polcar, T., & Cavaleiro, A. (2020). Comparative Study of DC and RF Sputtered MoSe2 Coatings Containing Carbon—An Approach to Optimize Stoichiometry, Microstructure, Crystallinity and Hardness. *THE Coatings, 10*, 133.

[31] Evaristo, M., Polcar, T., & Cavaleiro, A. (2009). Can WSeC Coatings Be Competitive to W-S-C Ones. *Plasma Processes and Polymers, 6*.

[32] Vuchkov, T., Yaqub, T.B., Evaristo, M., & Cavaleiro, A. (2020). Synthesis, microstructural and mechanical properties of self-lubricating Mo-Se-C coatings deposited by closed-field unbalanced magnetron sputtering. *Surface & Coatings Technology, 394*, 125889.

[33] Vuchkov, T., Evaristo, M., Yaqub, T.B., Polcar, T., & Cavaleiro, A. (2020). Synthesis, microstructure and mechanical properties of W–S–C self-lubricant thin films deposited by magnetron sputtering. *Tribology International, 150*, 106363.

[34] Mattox. (2010). Handbook of physical vapor deposition (PVD) processing (2nd ed.). Elsevier.

[35] Baptista, A., Silva, F.J., Porteiro, J., Míguez, J.L., & Pinto, G. (2018). Sputtering Physical Vapour Deposition (PVD) Coatings: A Critical Review on Process Improvement and Market Trend Demands. *Coatings*.

[36] Vuchkov, T., Yaqub, T.B., Evaristo, M., & Cavaleiro, A. (2020). Synthesis, Microstructural, and Mechano-Tribological Properties of Self-Lubricating W-S-C(H) Thin Films Deposited by Different RF Magnetron Sputtering Procedures. *Coatings*.

[37] Gustavsson, F., & Jacobson, S. (2016). Diverse mechanisms of friction induced self-organisation into a low-friction material – An overview of WS2 tribofilm formation. *Tribology International, 101*, 340-347.

[38] André, B., Gustavsson, F., Svahn, F., & Jacobson, S. (2009). Performance and tribofilm formation of a low-friction coating incorporating inorganic fullerene like nano-particles. *Surface & Coatings Technology, 206*, 2325-2329.

[39] Rapoport, L., Leshchinsky, V., Lapsker, I.A., Volovik, Y.I., Nepomnyashchy, O., Lvovsky, M., Popovitz-Biro, R., Feldman, Y., & Tenne, R. (2003). Tribological properties of WS2 nanoparticles under mixed lubrication. *Wear, 255*, 785-793.

[40] Gustavsson, F., Forsberg, P.K., & Jacobson, S. (2012). Friction and wear behaviour of low-friction coatings in conventional and alternative fuels. *Tribology International, 48*, 22-28.

[41] Gustavsson, F., Forsberg, P.K., Renman, V., & Jacobson, S. (2012). Formation of tribologically beneficial layer on counter surface with smart chemical design of DLC coating in fuel contact. *Tribology - Materials, Surfaces & Interfaces, 6*, 102 - 108.

[42] Vuchkov, T. (2020). *Upscale of magnetron sputtered TMD based thin films for tribological applications* (Doctoral dissertation).

[43] Ayerdi, J., Aginagalde, A., Llavori, I., Bonse, J., Spaltmann, D., & Zabala, A.M. (2021). Ball-on-flat linear reciprocating tests: Critical assessment of wear volume

determination methods and suggested improvements for ASTM D7755 standard. *Wear*, 203620.

[44] Petrov, I., Barna, P.B., Hultman, L., & Greene, J.E. (2003). Microstructural evolution during film growth. *Journal of Vacuum Science and Technology, 21*, 117.

[45] Voevodin, A.A., Fitz, T.A., Hu, J.J., & Zabinski, J.S. (2002). Nanocomposite tribological coatings with "chameleon" surface adaptation. *Journal of Vacuum Science and Technology, 20*, 1434-1444.

[46] Mutafov, P., Evaristo, M., Cavaleiro, A., & Polcar, T. (2015). Structure, mechanical and tribological properties of self-lubricant W–S–N coatings. *Surface & Coatings Technology, 261*, 7-14.

[47] Khalid, H. A. (2021). *Influence of N additions on the structure, morphology, thermal stability and tribological properties of WSN coatings deposited by sputtering* (Doctoral dissertation, Universidade de Coimbra).

[48] Sundberg, J., Nyberg, H., Särhammar, E., Gustavsson, F., Kubart, T., Nyberg, T., Jacobson, S., & Jansson, U. (2013). Influence of Ti addition on the structure and properties of low-friction W–S–C coatings. *Surface & Coatings Technology, 232*, 340-348.

[49] Evaristo, M., Azevedo, R., Palacio, C., & Cavaleiro, A. (2016). Influence of the silicon and oxygen content on the properties of non-hydrogenated amorphous carbon coatings. *Diamond and Related Materials, 70*, 201-210.

[50] Polcar, T., Evaristo, M., & Cavaleiro, A. (2007). The tribological behavior of W–S–C films in pin-on-disk testing at elevated temperature. *Vacuum, 81*, 1439-1442.

[51] Jacobs, R., Meneve, J., Dyson, G., Teer, D.G., Jennett, N., Harris, P.M., Stebut, J.V., Comte, C., Feuchter, P., Cavaleiro, A., Ronkainen, H., Holmberg, K., Beck, U., Reiners, G., & Ingelbrecht, C. (2003). A certified reference material for the scratch test. *Surface & Coatings Technology, 174*, 1008-1013.